Study of interaction and complete merging of binary cyclones using complex networks

Cite as: Chaos 33, 013129 (2023); doi: 10.1063/5.0101714
Submitted: 3 June 2022 · Accepted: 12 December 2022 ·
Published Online: 18 January 2023

Somnath De,[1,a)] Shraddha Gupta,[2,3,a)] Vishnu R. Unni,[4] Rewanth Ravindran,[1] Praveen Kasthuri,[1] Norbert Marwan,[2,5] Jürgen Kurths,[2,3] and R. I. Sujith[1]

AFFILIATIONS

[1]Department of Aerospace Engineering, Indian Institute of Technology Madras, Chennai 600036, India
[2]Potsdam Institute for Climate Impact Research (PIK)—Member of the Leibniz Association, Telegrafenberg A56, Potsdam 14473, Germany
[3]Department of Physics, Humboldt University at Berlin, Newtonstraße 15, Berlin 12489, Germany
[4]Department of Mechanical and Aerospace Engineering, Indian Institute of Technology Hyderabad, Kandi 502284, India
[5]Institute for Geosciences, University of Potsdam, Karl-Liebknecht-Straße 24-25, Potsdam 14476, Germany

Note: This article is part of the Focus Issue, Theory-informed and Data-driven Approaches to Advance Climate Sciences.
[a)]**Authors to whom correspondence should be addressed:** somnathde.mec@gmail.com and shraddha.gupta@pik-potsdam.de

ABSTRACT

Cyclones are among the most hazardous extreme weather events on Earth. In certain scenarios, two co-rotating cyclones in close proximity to one another can drift closer and completely merge into a single cyclonic system. Identifying the dynamic transitions during such an interaction period of binary cyclones and predicting the complete merger (CM) event are challenging for weather forecasters. In this work, we suggest an innovative approach to understand the evolving vortical interactions between the cyclones during two such CM events (Noru–Kulap and Seroja–Odette) using time-evolving induced velocity-based unweighted directed networks. We find that network-based indicators, namely, *in-degree* and *out-degree*, quantify the changes in the interaction between the two cyclones and are excellent candidates to classify the interaction stages before a CM. The network indicators also help to identify the dominant cyclone during the period of interaction and quantify the variation of the strength of the dominating and merged cyclones. Finally, we show that the network measures also provide an early indication of the CM event well before its occurrence.

In some active cyclone basins, more than one cyclone can be formed concurrently. Consequently, two or more cyclones can come in close spatial proximity and start interacting with each other; this type of interaction is known as the "Fujiwhara interaction." Such an interaction may lead to many possibilities, such as weakening of both cyclones, sudden alteration in their tracks, re-strengthening of one of the cyclones due to vorticity interaction, and, very rarely, the birth of a more intense long-lived cyclone due to complete merging between them. This binary interaction between cyclones has not been fully understood and remains a major challenge for weather forecasters. This often leads to inaccurate predictions, increasing the risk of human life and property due to unpreparedness. Most previous investigations have used the separation distance between the cyclones to classify the stages of binary interaction leading to merging and to predict their merger. However, the separation distance between the cyclones does not only influence the Fujiwhara interaction but also depends on it. In particular, the Fujiwhara effect may alter the track of cyclones, leading to elastic interaction, partial straining out, or the partial merger between two cyclones. As a result, characterizing the behavior of binary cyclones based on the separation distance may be difficult. In this study, we use a novel approach based on complex networks. We analyze the vortical interactions in the spatial domain by constructing time-evolving induced velocity networks. Using two prominent examples of complete merger events, namely, the Seroja–Odette and Noru–Kulap interactions in the Northern and Southern Hemispheres, respectively, we show that network-based measures are successful in classifying the binary interaction stages.

I. INTRODUCTION

Cyclones are organized non-frontal synoptic convective vortical systems that are formed over tropical or subtropical waters. Essentially, they are characterized by a low-pressure center[1] that produces strong surface wind circulation. When a cyclone makes landfall, torrential rains and the accompanying strong winds impart severe widespread damage to land infrastructure, disrupting human lives and even resulting in numerous casualties. The massive destruction caused by severe cyclones in recent years has raised serious concerns that these extreme weather events may be a consequence of human-induced climate change. Due to global warming, sea surface temperatures have risen, and the maximum capacity of the atmosphere to hold water vapor has also increased. A number of studies[2] have indicated that anthropogenic global warming is likely to cause an increase in the intensity of cyclones, higher precipitation rates, and elevated storm surge risks. Tropical cyclones may also intensify more rapidly, have slower translation speeds, and occur at higher latitudes.[2] Therefore, understanding the behavior of cyclones is of utmost interest to weather forecasters and policymakers.

In some very active cyclone basins, such as the Northwestern Pacific and Atlantic, multiple cyclone systems can be formed simultaneously. Although rare, two cyclones can come within close proximity and interact, beginning an intense dance about their common center. This may lead to the strengthening of the cyclones, sudden track changes, or even the complete merger of one cyclone into the other. Such an interaction of binary cyclones was first reported by Okada.[3] According to his observation, cyclones tend to come closer and intensify if they spin in the same direction, while they tend to separate if they rotate in the opposite direction. Later, Fujiwhara made similar deductions on the amalgamation of cyclones through laboratory experiments and geophysical observations.[4–6] Subsequently, this binary cyclone interaction, when two cyclones make a close pass, came to be known as the "Fujiwhara effect." Thereafter, a number of weather events have been recorded where one cyclone has been observed to interact with another cyclone within close proximity.[7–9]

The Fujiwhara interaction often alters the tracks of the cyclones, making them difficult to forecast. Inaccuracies in predicting cyclone tracks increase the threat to life and property due to unpreparedness caused by misinformation and the lack of early warning. For instance, unforeseen heavy rainfall occurred in Taiwan, and the same region of the Luzan Island of the Philippines experienced landfall of typhoon Parma thrice due to its interaction with another typhoon Melor in October 2009, causing significant fatalities and economical losses.[10] In most cases, the Fujiwhara effect weakens both cyclones as the winds involved with cyclones in the same hemisphere during the interaction tend to blow opposite to each other. However, very rarely, the binary interaction may lead to re-strengthening of the cyclone, as in the case of Category 3 severe tropical cyclone Seroja in April 2021 due to its complete merger with Odette.[11] Interaction of a cyclone with other cyclonic vortices may also prolong its life span; e.g., the Super Typhoon Noru in July 2017 lasted for 19 days due to its successive dual vortex direct and indirect interactions with typhoons Kulap, Haiting, and Nesat.[12] To date, a complete understanding and incorporation of the Fujiwhara effect in numerical weather prediction models to improve cyclone forecasts have not been achieved. Hence, understanding cases of binary cyclone interaction remains highly relevant.

Generally, based on a circulation-based vortex pair interaction, the interaction of cyclones is classified into five categories,[13] which are (a) partial straining out, (b) complete straining out, (c) partial merger, (d) complete merger, and (e) elastic interaction. (a) and (c) signify the partial deformation of the interacting pair, while complete deformation of one of the interacting vortices can be found in (b) and (d). In (e), each interacting vortex survives, although its direction of motion changes. Among them, a complete merger (CM) of two cyclones is of great interest to the meteorologists because it is one of the most complicated interactions in the context of the transfer of energy and vorticity across the turbulent flow scales.[14] Earlier studies[14–16] based on theoretical calculations have shown that the diffusion of vorticity from the inner core region to the inner and outer recirculation regions in a system of co-rotating vortices was the reason for their merging. However, such inner- and inter-layer fluid exchanges are not confirmed in real-world binary cyclone interactions.

As a result, forecasting cyclone tracks when two low-pressure systems are in close spatial proximity is a challenging task. One of the important factors related to the error in the forecasts of the cyclone tracks is the presence of another low-pressure system in close spatial proximity.[17–20] Several studies[9,17,21,22] based on observational data found that although most mutual interactions close to the intertropical convergence zone (ITCZ) in the North Pacific agree with the Fujiwhara expectations, there were some notable exceptions, especially in the North Atlantic. Moreover, Lander and Holland[22] in their detailed analysis on interacting cyclonic vortices in the western North Pacific found that the classical Fujiwhara model of CM is seldom followed. They reported that the presence of large-scale clockwise circulation patterns masks the Fujiwhara effect, sometimes even at separation distances where the Fujiwhara forces are quite strong. Furthermore, large-scale circulation due to the presence of subtropical high or monsoon depression[22–25] and the presence of multiple weak cyclonically rotating meso-vortices[20] pose significant challenges toward cyclone track forecasts. Therefore, weighing the impact of binary interaction on cyclone track and intensity is essential to cyclone forecasters.

Several numerical and analytical studies on the interactions of binary cyclones have been attempted in an effort to understand both two-dimensional[7,8,10,14] and three-dimensional dynamics[26,27] of the CM phenomena. Most of them underlined the significant role of the separation distance in the interaction between binary cyclones. Wei-Jen Chang[26] showed an agreement with Fujiwhara's description of CM in the absence of large-scale circulations using a three-dimensional cyclone model. His investigation also showed that the displacement of one of the interacting cyclones in the mutual rotation is proportional to the combined strength of the binary system but is inversely proportional to the size of the cyclone and to the square of the separation distance. On the contrary, their simulations using the non-divergent barotropic model in which the vortices interact by advection alone showed no signs of mutual attraction. However, DeMaria and Chan[27] later demonstrated that the mutual attraction can be explained using vorticity advection alone and is strongly dependent on the initial wind profile of the vortices. A number of studies[17,28–32] found that merging occurs when the sizes

of the vortex cores of co-rotating vortices increase beyond a critical fraction of the separation distance due to viscous diffusion. Furthermore, several dissipative and convective stages[16,33] are identified based on the separation in the vortex merging process. Such an occurrence of a rapid merger following the approach of cyclone-scale vortices within a critical separation distance was reported from simulations[22,24,34] of a modified model of binary interaction. However, there have not been much investigations on the dynamics of CM based on observation or reanalysis data to compare with these model-based findings.

Despite the numerous studies on the shearing of cyclones when in close proximity,[10,35,36] the interaction of two neighboring cyclones before a CM is not well explored due to the paucity of the occurrence of such merging events in nature. To that end, in the current study, we select two recent binary cyclone systems—Noru–Kulap (during 23–26 July 2017)[12,37] occurring in the Northern Hemisphere and Seroja–Odette (5–10 April 2021) in the Southern Hemisphere—which engaged in a Fujiwhara interaction and exhibited a CM event. The Category 4 Super Typhoon Noru, the third longest-lived cyclone on record in the Northwest Pacific Ocean, became the second most intense tropical cyclone of the Northwestern Pacific Ocean basin in 2017 due to Fujiwhara interaction with Kulap and indirect interactions with other cyclone systems.[12] Noru brought torrential rainfall to southern and western parts of Japan that triggered widespread flooding and caused large economic losses.[38] Similarly, following the interaction of the severe tropical cyclone Seroja with the tropical storm Odette, the CM event steered the merged cyclone southward toward Australia and further strengthened it, as mentioned earlier. Then, the merged cyclone made landfall on the west coastline of Western Australia as a Category 3 severe tropical cyclone causing significant damage. Its prolonged southward trajectory was highly unusual as cyclones of similar intensity have traveled so far south only 26 times in the past 5000 years.[11,39] In view of the aforementioned discussion, we need an approach that enables us to gain deep insights into the dynamics of such a highly complex weather system.

In recent decades, complex network theory has emerged as one of the most powerful tools in understanding the interactions between the different units of a complex system across various disciplines.[40–45] Tsonis *et al.*[46] first applied this theory to study climate by considering the climate system to be represented by a grid of oscillators interacting with each other in a complex way, with each one representing climate variability of a particular location of the gridded spatiotemporal dataset. Since then, the network representation of spatiotemporal climate data has been very successfully applied to study different climate and weather phenomena.[47–59]

Recently, Gupta *et al.*[60] used time-evolving complex networks of mean sea level pressure (MSLP) data to study cyclones in the North Indian Ocean and tropical North Atlantic Ocean basins. They demonstrated that network-based indicators can be used to characterize the topological evolution of the regional climate system during highly localized weather extremes, which occur over short time scales, such as cyclones and detect cyclone tracks, besides climate phenomena, such as monsoon and the El Niño–Southern Oscillation (ENSO) that occur over seasonal or annual time scales.

In the present work, we study the vortical interactions between two cyclones in close proximity leading to a CM under a novel framework based on time-evolving induced velocity-based unweighted networks. The adoption of an induced velocity network based on the Biot–Savart law has been successfully used to study the turbulent flow dynamics.[61] Here, we extend the methodology to investigate flow dynamics in cyclonic systems (refer Sec. II B). In contrast to the correlation-based networks,[60,62] which depict only statistical relationships, the induced velocity networks represent real physical links, indicating the induction of velocity by one flow element on the others. By considering the instantaneous vorticity field as a directed spatiotemporal network, we compute network measures, such as the *in-degree* and the *out-degree*, which count the number of links going to and arising from a particular grid point (see Sec. II C). This enables us to track the changes in the interaction zone of the binary cyclone system at every instant, as they approach each other, instead of performing a time-averaged analysis over the whole lifespan of the cyclones as done by Gupta *et al.*[60] We find that changes in the *in-degree* reflect the variations in the nature of the interaction between two cyclones, while those in the *out-degree* are indicative of the vortical interactions within a cyclone. Our results show that as the two cyclones approach each other, the ensuing changes in the network topology can be used to classify the complete merging process into several interaction stages. We find that this approach helps to characterize the evolution of the cyclones[60] in a binary cyclone system as well as quantifies the mutual interaction when they are in the close vicinity of each other[17,28,29] and gives an early indication of the occurrence of CM. Significantly, the proposed network-based measures are effective in identifying the disparity in the interaction stages between two binary cyclone systems considered in the study.

The rest of this paper is organized as follows. In Sec. II, a detailed description is provided about the source of data and the method of the construction of the network, which is used in the present study. In Sec. III A, we perform a spatial analysis based on network measures, such as *in-degree* and *out-degree*, to understand the temporal evolution of vortical interactions between the two converging cyclones. In Sec. III B, we find the transitions exhibited by the maximum *in-degree* and the *out-degree* of the time-evolving networks, which enable us to classify the stages of the mutual interaction and merging between two cyclones. Finally, the significant conclusions from the study are summarized in Sec. IV.

II. METHODOLOGY

A. Reanalysis dataset

In the present work, we use the relative vorticity (ω) data obtained from the state-of-the-art ERA5 reanalysis dataset[63] to understand the interaction dynamics between two co-rotating cyclones. Relative vorticity is defined as the rotation of air about a vertical axis, relative to a fixed point on the Earth's surface and calculated as $\omega = \frac{\partial v}{\partial x} - \frac{\partial u}{\partial y}$, where u and v correspond to the velocity along x (longitude) and y (latitude), respectively.

Relative vorticity is reported to be more suitable than the mean sea level pressure (MSLP) field for capturing the local features in the evolution of cyclones. The features of small-weak circulations (for example, during the onset of a cyclone) are not adequately

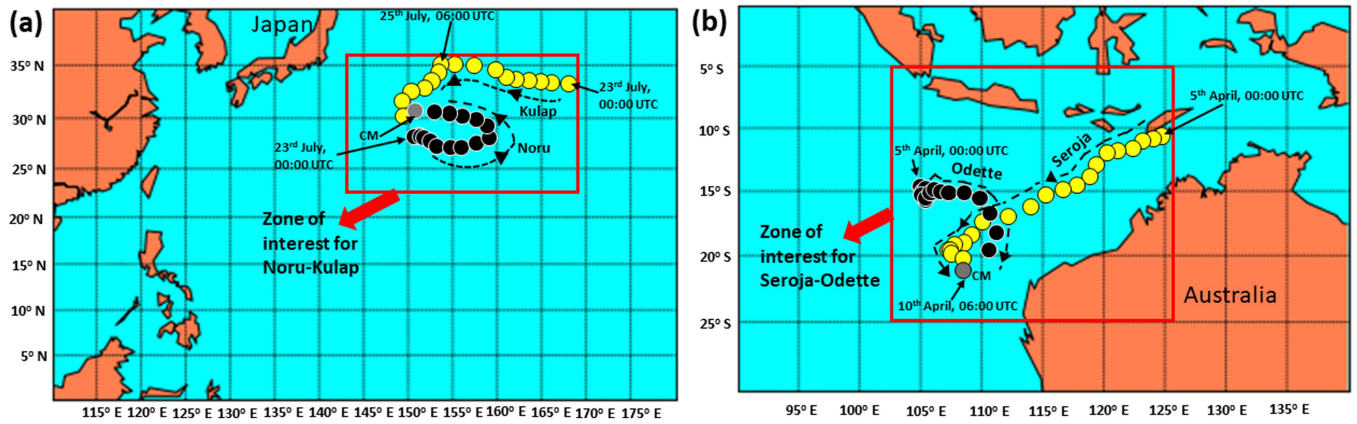

FIG. 1. The regions of interest considered for the network during (a) Noru–Kulap and (b) Seroja–Odette interactions are shown. In the case of the Noru–Kulap interaction, the area extends from 143 °E to 169.5 °E and from 23.5 °N to 35.5 °N. For the Seroja–Odette interaction, the region of interest extends from 102 °E to 125.5 °E and from 5 °S to 25 °S. The trajectories of the cyclones at time steps of 6 h are also shown to visually justify the selection of the spatial domain.

represented in the MSLP field as compared to that in the relative vorticity field at 850 hPa.[64,65] Furthermore, large-scale relative vorticity at lower atmospheric levels (500–850 hPa) is known to significantly affect cyclones[66–68] and influence their relative motion in the presence of another cyclone.[21] Many previous studies[7,10,26,35] on binary cyclone interaction found it difficult to correctly incorporate these large-scale circulations in cyclone models, leading to erroneous predictions of cyclone tracks. The use of relative vorticity from reanalysis data ensures the inclusion of these large-scale wind circulations.

As the probability of detecting cyclones improves with an increase in spatial resolution[69] and also that the relative vorticity, being a wind-based field, is sensitive to the spatial resolution of the data set,[65] we use a high spatial resolution of $0.5^\circ \times 0.5^\circ$ for our analysis. For the analysis of the Noru–Kulap interaction, the spatial region of interest extends from 143 °E to 169.5 °E and from 23.5 °N to 35.5 °N [Fig. 1(a)]. Similarly, in the case of the Seroja–Odette interaction, the spatial region of interest extends from 102 °E to 125.5 °E and from 5 °S to 25 °S [Fig. 1(b)]. The spatial domain is chosen in a manner that ensures the elimination of any other neighboring weaker cyclonic or anticyclonic vortices apart from the considered cyclone pair. Therefore, inherently, we have made the assumption that the cyclone pair is not affected by the climate behavior outside the selected spatial region. Furthermore, in order to study the rapid intensification and weakening of the cyclones and the changes in their mutual interactions, we use a temporal resolution of 3 h for the relative vorticity data set, as often used by cyclone track forecasters.[60,70]

We perform our analyses to obtain the interaction structure of the two-dimensional relative vorticity field at the lower tropospheric level of 850 hPa, as commonly used for cyclone forecasts.[71,72] Vorticity at 850 hPa has a stronger magnitude compared to vorticity at near surface heights (1000 hPa), especially for weaker circulations, and, therefore, is more robust when representing the strong upward motion of air. Hence, the 850 hPa relative vorticity field exhibits better continuity in the course of cyclone evolution,[64] which is essential to deal with a CM event of two cyclones. Moreover, weaker cyclones have a shallow-lower tropospheric vertical depth (850–500 hPa), while only the most intense cyclonic systems move with a deeper layer flow (850–200 hPa),[73,74] which should be taken into account for producing optimal forecasts of cyclone tracks with the lowest mean forecast errors.[75] Therefore, we also investigate the evolution of the network connectivity structure for other higher tropospheric levels (650 and 700 hPa) such that it includes most cyclones, which not only allows us to verify the consistency of our results, but also to identify the transitions in the interaction structure of the binary cyclone system in the three-dimensional column of the atmosphere.

B. Construction of time-evolving directed networks

The interactions between the different components of a complex system can be represented as a complex network in which each component can be considered a node, and the pairwise interactions between the different components are represented as links between the nodes. Since its inception, complex network has been extensively followed to understand the collective behavior of many real-world complex systems.[46,48,76–83] In the current work, we use a network-based approach to study the two-dimensional vortical interactions in binary cyclone systems at a particular geopotential height. Each grid point (Fig. 2) is considered a node, and the links between two nodes represent the interaction between the fluid elements at the corresponding grid points.[45,61,84] In order to calculate the interaction between fluid elements, we use the Biot-Savart law. It is widely used to calculate the magnetic field induced by a current-carrying wire in electromagnetic theory[85,86] and aerodynamic forces exerted by the flow on complex geometries, such as wings using vortex panel methods.[87]

In this study, we use the Biot-Savart law to primarily estimate the weight of the connection between any two points in the flow field. Strictly, the Biot-Savart law is only applicable for incompressible flows, that is, when the velocity field is divergence-free. The velocity field associated with cyclonic flows is not divergence-free

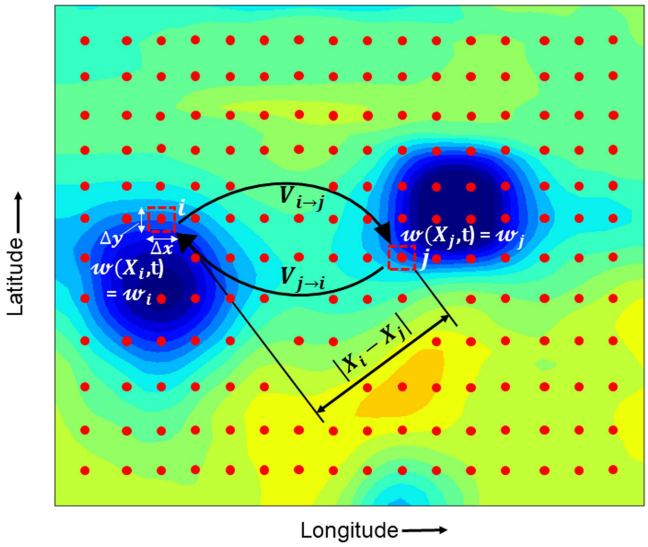

FIG. 2. Schematic illustration of the method of construction of a vorticity network for a binary cyclone system at a particular time step *t*. The solid red circles in the spatial domain represent the grid points or nodes. The velocity, induced by the flow element at node *i* on node *j*, is shown in terms of $V_{i\to j}$. Similarly, $V_{j\to i}$ indicates the induced velocity on the *i*th element by the *j*th element. ω_i and ω_j represent the relative vorticities at *i*th and *j*th flow elements, respectively. The dashed square boxes represent the size of the fluid elements at the *i*th and *j*th grid points.

especially close to the center of the cyclone. Therefore, the value of the induced velocity found using this method is not necessarily accurate at all points but is adequate to compare the strength of connections between different spatial locations.

Following the Biot-Savart law, we estimate the magnitude of the velocity induced by the vorticity of a flow element at the *i*th grid point on another flow element at the *j*th grid point ($V_{i\to j}$) (Fig. 2)[85] as

$$V_{i\to j} = \frac{|\gamma_i|}{2\pi\,|X_i - X_j|}, \tag{1}$$

where X_i and X_j are the spatial location of the *i*th and *j*th grid point, respectively. We take the absolute value of the circulation [$\gamma_i = \omega(X_i)\Delta x\Delta y$] of the flow element at the grid point (node) *i* as mentioned in Taira *et al.*[61] Treating the spatial domain as planar (2D), we compute the Euclidean distance between the *i*th and *j*th nodes represented by $|X_i - X_j|$. If the number of grid points (nodes) in the flow domain is *N*, then the size of the induced velocity matrix is $N \times N$. The velocity induced by the flow element at the *i*th node on the element at the *j*th node ($V_{i\to j}$) is different from that induced by the element at the *j*th on the element at the *i*th node ($V_{j\to i}$), and therefore, the matrix is asymmetric.

Furthermore, following previous studies,[52,60] we consider only the highest 5% of the induced velocities to define the links in our network. This 95th percentile of the induced velocity is found to be the optimum choice to retain connections corresponding to both cyclones, ensuring that the network is not too dense. Then, we build an adjacency matrix by registering the connections with links by 1. The rest of the elements of the adjacency matrix are filled by zeros. We also neglect self connections; i.e., the velocity induced by a flow element on itself is considered to be zero [Eq. (2)]. Thus, we construct an unweighted directed network whose adjacency matrix A_{ij} is represented as

$$A_{ij} = \begin{cases} 1 & \text{if } i \neq j \text{ and } V_{i\to j} > \text{threshold}, \\ 0 & \text{otherwise.} \end{cases} \tag{2}$$

In this manner, we construct a time-varying spatial network from the vorticity field at every time instant to understand the evolution of the binary cyclone interaction.

In relevance to the current study, Gupta *et al.*[60] used a correlation-based network spanning over a time window of 10 days, which encoded the interactions in the spatiotemporal field of MSLP data, to detect cyclone track in the basin. However, such a time-averaged network is unable to capture the evolution of a mutual interacting binary cyclone system, which varies over hourly to daily time scales. Therefore, instantaneous time-varying vorticity networks are a better alternative to not only detect cyclones but also to study their interaction with other cyclones.

C. Network measures

In this analysis, we measure the strength of the nodes in the interacting flow domain through the network measure, degree,[44] which counts the number of links or connections a node has with others. As our instantaneous vorticity network is a directed network, we distinguish the number of incoming and outgoing links to and from a node in terms of its *in-degree* (k_i^{in}) and *out-degree* (k_i^{out}), respectively.[44] k_i^{in} is defined as

$$k_i^{in} = \sum_{j=1}^{N} A_{ji}, \tag{3}$$

and represents the *in-degree* of the flow element at the *i*th node, where $i \neq j$. Through k_i^{in}, we can describe the impact of the induced velocities of the neighboring nodes at the *i*th node in the interaction domain.

On the other hand, k_i^{out} is defined as

$$k_i^{out} = \sum_{j=1}^{N} A_{ij}, \tag{4}$$

and represents the number of outgoing links from the flow element at the *i*th node, where $i \neq j$. k_i^{out} can identify the strong vortices, which induce velocities over a long distance in the interaction domain.

D. Separation distance between cyclones

The separation distance is the widely used metric to classify the interaction stages of binary cyclones[22,34] and the vortex merging process.[16] In the present study, the position of each cyclone is tracked on the basis of the geographical latitude and longitude of the center, obtained from Weather Underground's online database.[88] We use the Haversine formula[89] to calculate the separation distance (*d*) between two cyclones. The steps used in this calculation are given in the Appendix.

III. RESULTS AND DISCUSSION

First, we describe the evolution of the network connectivity structure of the two binary cyclone systems and try to relate it with the changes observed in their relative vorticity field (Sec. III A). Thereafter, in Sec. III B, we use the transitions obtained from the network-based parameters to classify the merging process into different stages.

A. Degree analysis on the vorticity network

1. Noru–Kulap interaction

We investigate the binary interaction between Noru and Kulap and the effect of neighboring air flows in Northwest Pacific[12] during July 2017. The strong positive values in the relative vorticity distribution signify the rising motion of air causing the winds to be deflected counterclockwise, as is typical for Northern Hemisphere cyclones[90] [Figs. 3(a1)–3(d1) and 4(a1)–4(d1)]. During the period between 23 July and 24 July 2017, Kulap is observed to change its track slightly toward the west, while a bit of eastward movement is seen in Noru.[37] After that, from 25 to 26 July 2017, a significant change in the direction of their movement results in a reduction of separation distance (d). Here, first, we discuss the interaction of these two cyclones during the period of 23 July–24 July 2017 (Fig. 3).

On 23 July, Kulap and Noru are far apart from each other [$d \sim 1510$ km, Fig. 3(a1)]. From the network structure, at this stage, we find a higher k^{in} at the region closer to the center of Kulap compared to that of Noru, which signifies a dominating vortical influence from other regions on Kulap [see Fig. 3(a2)]. As also indicated from the higher k^{out} values within Noru than Kulap [see the center of two cyclones in Fig. 3(a3)], the vortical influence of Noru on Kulap dominates at this period. It is seen that, initially, k^{in} is very low in the region between these two cyclones. As the cyclones rotate about each other, k^{in} gradually increases in that region [see Figs. 3(b2)–3(d2)]. This increase in k^{in} is due to the vorticity exchange[16] between the cyclones, which is prominently observed on 24 July 12:00 UTC [cf. Fig. 3(d1)]. On the other hand, the outer layers of Kulap facing Noru have comparatively higher k^{in} than that of Noru facing Kulap,

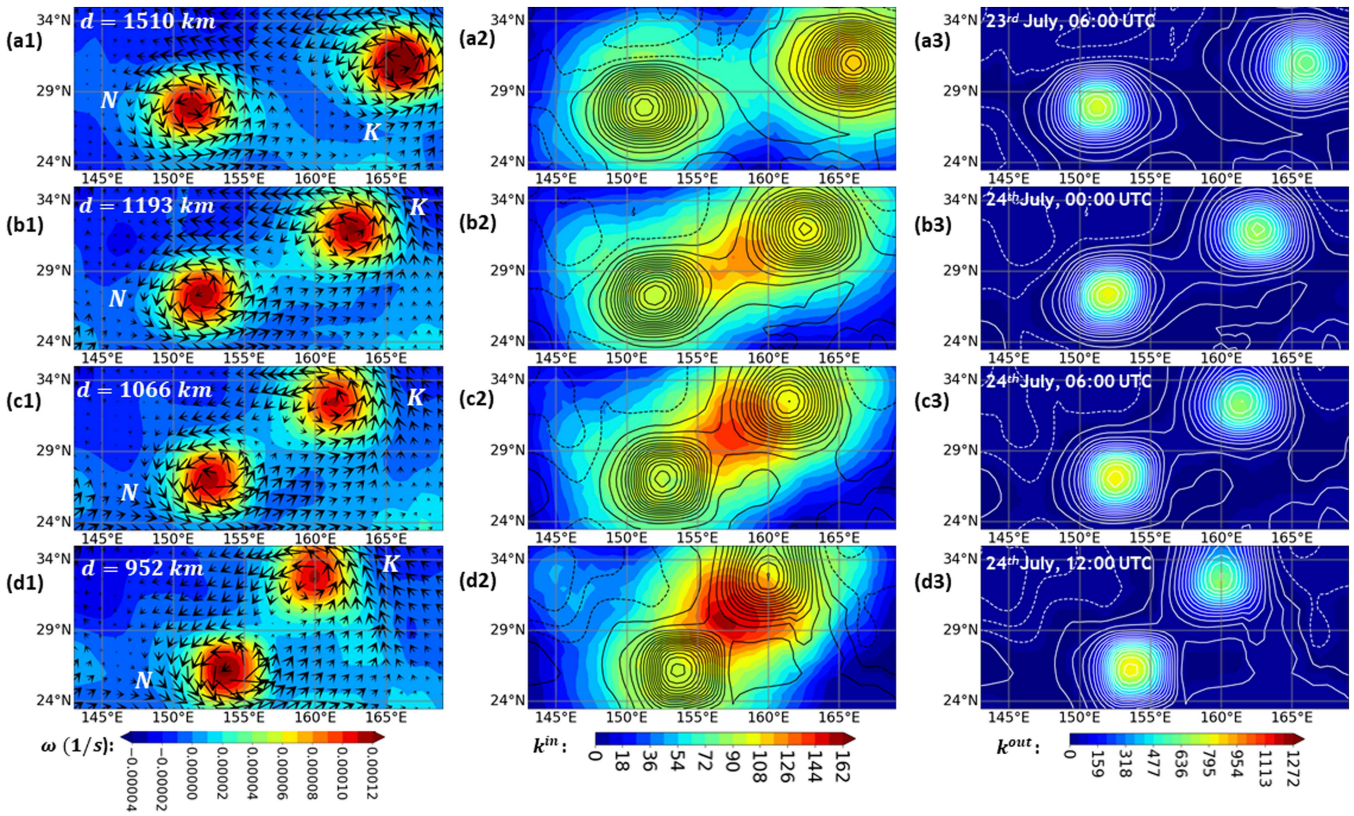

FIG. 3. The distributions of ω (a1)–(d1), k^{in} (a2)–(d2), and k^{out} (a3)–(d3) are presented during the interaction of Noru (N) and Kulap (K) at a geopotential height of 850 hPa during the period of 23–24 July 2017. The time steps shown here are (a1)–(a3) 23 July 2017, 06:00 UTC; (b1)–(b3) 24 July 2017, 00:00 UTC; (c1)–(c3) 24 July 2017, 06:00 UTC; and (d1)–(d3) 24 July 2017, 12:00 UTC. The velocity vector of the wind is shown in (a1)–(d1). The vorticity contours of (a1)–(d1) are shown in the distribution of k^{in} and k^{out} for better understanding the changes of Noru–Kulap interaction. Note that the positive vorticity is represented by the solid lines, while dotted lines in vorticity contour indicate the negative vorticity. During the vorticity exchange between two cyclones, k^{in} increases significantly between two cyclones. The higher k^{out} at the center of Noru indicates its strong impact on the neighboring nodes.

which also signifies the higher impact of Noru on Kulap [see the higher k^{in} between two cyclones in Figs. 3(b2)–3(d2)]. Besides, the distributions of k^{out} of the two cyclones highly resemble the vorticity distributions ($a3$–$d3$ of Fig. 3) with the highest k^{out} at the center of the cyclones. A significant decrease in k^{out} is noticed as we move away from the center of the cyclone toward its outer layers.

In addition, we find a sudden drop of k^{out} outside a certain radius, indicating the presence of higher interacting nodes inside the cyclones. Higher k^{out} values at the nodes of Noru than those of Kulap within 23 and 24 July 2017 corroborate the same understanding that the vortical influence of Noru highly dominates over that of Kulap on other nodes. Also, the vortical influence of the non-cyclone nodes has minimal effect compared to the cyclones, as seen from their near zero k^{out} values. Thus, the higher k^{in} during the inter-layer vorticity exchange between two cyclones confirms that the vortical influences at that zone mainly come from Noru.

Furthermore, during the period 25–26 July 2017, Noru turns first to the north and then west, while Kulap turns to the southwest[37] [Figs. 4(a1)–4(d1)]. During this time, the vorticity core of Kulap is observed to diminish as the inter-layer vorticity interaction between the two leads to the formation of an unstable connected structure[91] [Figs. 4(b1)–4(c1)]. The corresponding k^{in} distribution shows a significant shrinkage in the area covered by higher k^{in} between both cyclones (comparing $b2$–$d2$ with $a2$ in Fig. 4). During this period, due to the closer proximity of Noru and Kulap, the interaction between them reduces significantly. A similar region of high k^{in} but of relatively less magnitude is seen on the side of Noru opposite to that of Kulap [Fig. 4(b2)], which subsequently diminishes [Figs. 4(c2)–4(d2)]. This additional k^{in} region can be attributed to Noru's interaction with a neighboring weak vortex (at around 26 °N, 162 °E) [Figs. 4(c1)–4(d1)], which is not of interest in our present work. On the other hand, a significant simultaneous reduction and increment of k^{out} of Kulap and Noru, respectively, happen when $d \sim 800$ km [Fig. 4(a3)]. During the complete merging, when Kulap moves toward Noru, k^{out} at the location of Kulap reduces to almost zero [see Figs. 4(c3)–4(d3)].

In a nutshell, k^{in} provides a quantitative measure of the binary interaction through vorticity advection between Noru and Kulap. In

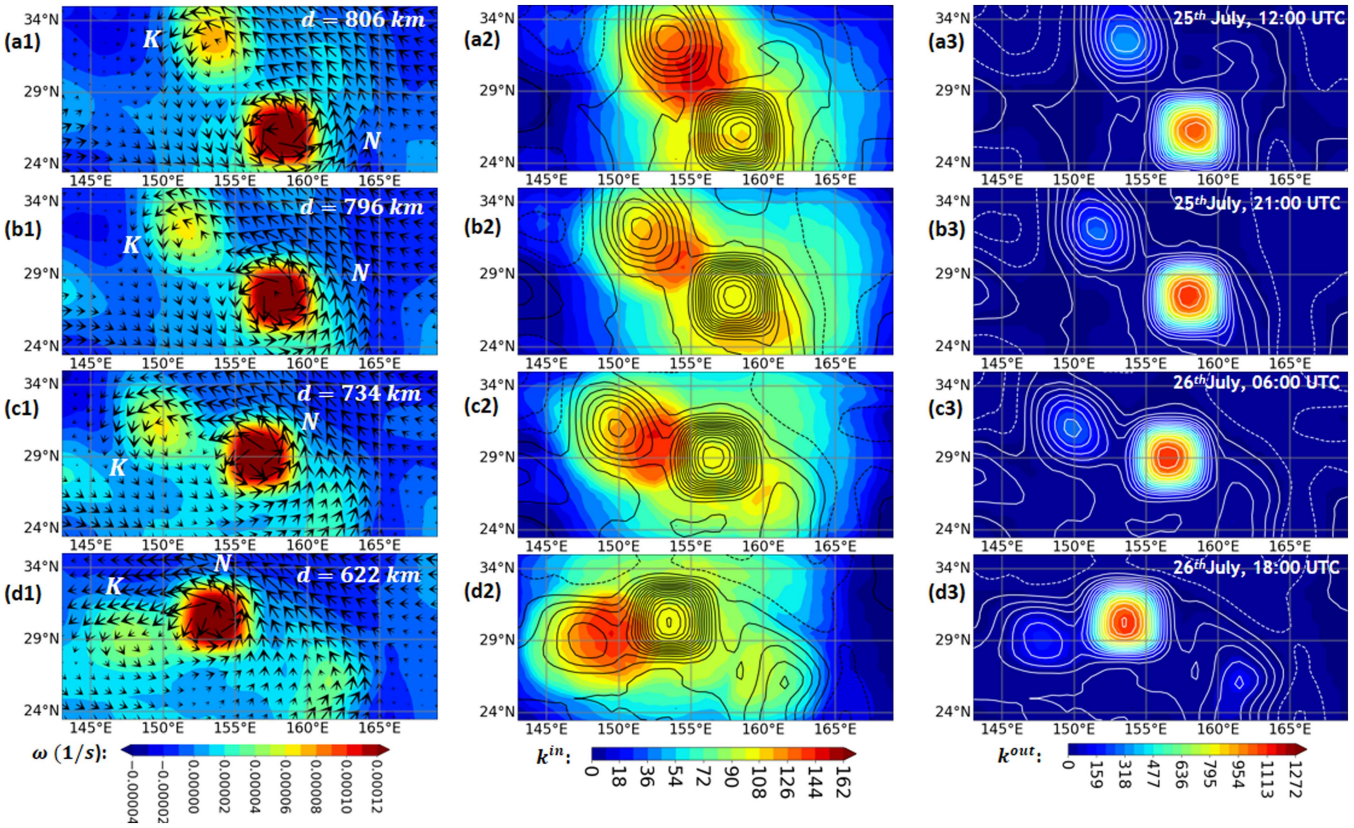

FIG. 4. The distributions of ω (a1)–(d1), k^{in} (a2)–(d2), and k^{out} (a3)–(d3) are presented during the interaction of Noru (N) and Kulap (K) prior to their merging at a geopotential height of 850 hPa during the period of 25–26 July 2017. The time steps shown here are (a1)–(a3) 25 July 2017, 12:00 UTC; (b1)–(b3) 25 July 2017, 21:00 UTC; (c1)–(c3) 26 July 2017, 06:00 UTC; and (d1)–(d3) 26 July 2017, 18:00 UTC. We can see closer proximity between two cyclones (a1)–(d1) before the merging. Besides, the reduction and increment of k^{out} at the center of Kulap and Noru, respectively, help to understand the merging after a vorticity exchange happens between them. The vorticity contours of (a1)–(d1) are shown in the distributions of k^{in} and k^{out}.

contrast, the dominating influence of Noru over Kulap is captured through k^{out} at each time instant.

2. Seroja–Odette interaction

First, we present the relative vorticity field at 850 hPa [Figs. 5(a1)–5(d1)] and the corresponding spatial distributions of k^{in} [Figs. 5(a2)–5(d2)] and k^{out} [Figs. 5(a3)–5(d3)] during the interval from 6 April 2021, 06:00 UTC to 8 April 2021, 09:00 UTC of the interacting period between Seroja and Odette in Fig. 5. In contrast to the Noru–Kulap interaction, strong negative values of ω [Figs. 5(a1)–5(d1) and 6(a1)–6(d1)] indicate a strong upward movement of air, causing the winds to rotate in a clockwise motion (as shown by the wind velocity vector), typical of cyclones in the Southern Hemisphere.[92] From Figs. 5(a1)–5(d1), we find two distinct regions of negative ω values (blue color) in the vorticity field, indicating two cyclones. The vortex on the right side of the window represents cyclone Seroja (marked *S*),[93] whereas the vortex on the left side is the cyclone Odette (marked *O*). On 6 April at 06:00 UTC, these two cyclonic systems were ∼1690 km apart [Fig. 5(a1)]. Around this time, vorticity diffuses from the "inner core" (i.e., the intensified vorticity zone at the center of the cyclone) to the outer layers (i.e., the surroundings of the center) of the cyclones, dynamically changing the shape of the cyclones.[14] This phenomenon has been referred to as the intra-layer vorticity exchange.[14]

Odette stays almost at the same location throughout the interacting period, from 6 April to 7 April 2021 [Figs. 5(a1)–5(c1)]. In stark contrast, Seroja continuously moves toward Odette. As a consequence of this rapid movement of Seroja, d significantly reduces [Figs. 5(a1)–5(c1)] during the interacting period. The detailed quantification of d during this interaction is discussed later in Sec. III B.

From the network connectivity structure, initially, we find that k^{in} at the grid points inside Odette is relatively larger than those inside Seroja [Fig. 5(a2)] for a higher value of d. The higher k^{in} inside Odette denotes a higher vortical influence on the nodes of that regime by the other long-range or nearby nodes. On the other hand, k^{out} is always observed to be higher inside the cyclones than the non-cyclonic regions in the spatial domain [Figs. 5(a3)–5(d3)], implying high outgoing links from the cyclones. As the vorticity diffusion occurs from the center to the outer layers of the cyclone and is limited to its outermost layer, we find a similar drop of k^{out} beyond a certain radius of the cyclone as compared to the Noru–Kulap interaction (Figs. 3 and 4). Furthermore, the k^{in} values are ∼ 10 times lower than the k^{out} values, which indicate that the number of links connecting both cyclones is comparatively less than the links arising from a cyclone.

Similar to the Noru–Kulap interaction, as d reduces, the area covered by the higher k^{in} nodes is observed to increase in between both cyclones [Figs. 5(b2)–5(d2)]. After 2 days, when $d \sim 812$ km, the significantly higher k^{in} between the cyclones [Fig. 5(d2)] implies higher incoming links from the surrounding regions, thereby indicating that the vortical interactions occurring between both cyclones are very high. This high vorticity exchange[16] occurs through the establishment of an inter-layer vorticity diffusion [Fig. 5(d1)]. Interestingly, compared to Seroja, Odette is closer to the higher k^{in} area [see the contours of vorticity of the cyclones in Figs. 5(b2)–5(d2)] for lower values of d. In contrast, we find higher k^{out} values at the grid points inside Seroja than Odette [Figs. 5(a3)–5(d3)]. However, there is a slight drop in the magnitude of k^{out} at the core of Seroja during inter-layer diffusion. All these observations suggest that Seroja exhibits more influence on the intermediate region than Odette during their interaction [Figs. 5(a3)–5(d3)]. However, from the establishment of inter-layer diffusion to the near CM event, we find a significant difference in ω and k^{out} between Noru and Kulap, which is higher than that observed between Seroja and Odette. The increasing rate of vorticity absorption of Noru from Kulap during this phase is the primary reason for that.

Furthermore, we show the distributions of ω [Figs. 6(a1)–6(d1)], k^{in} [Figs. 6(a2)–6(d2)], and k^{out} [Figs. 6(a3)–6(d3)] of the Seroja–Odette interaction during the interval from 8 April 2021, 12:00 UTC to 10 April 2021, 06:00 UTC in Fig. 6. After the establishment of inter-layer diffusion, the inner core of Odette moves toward Seroja [in Fig. 6(b1)]. Thus, we observe a dumbbell-shaped connected cyclonic structure[91] at this stage. Besides, during this stage of interaction, k^{in} significantly shrinks within these connected cyclones [Fig. 6(b2)], which signifies that the vortical influence from the cyclones on the interacting zone becomes lower compared to that found on 8 April 2021, 12:00 UTC [see Fig. 6(a2)]. On the other hand, the k^{out} distribution of the cyclones [see Fig. 6(b3)] bears a good resemblance to the corresponding vorticity distribution [Fig. 6(b1)]. At this time, k^{out} of the core of Seroja intensifies further due to the intake of vorticity from Odette.

After 3 days, cyclone Odette decays, as indicated by the lower magnitude of negative ω [Fig. 6(c1)]. In the next stage ($d1$ in Fig. 6), we see only a single vortex in the window, which confirms the occurrence of binary cyclone merging. The area covered by the higher k^{in} is also observed to shrink simultaneously ($d2$ in Fig. 6) during the CM event. Besides, we observe a higher k^{out} at the center of cyclone Seroja, while the region of high k^{out} abruptly vanishes around Odette ($d3$ in Fig. 6).

Nevertheless, the topology of the interaction between the cyclones in Secs. III A 1 and III A 2, as the cyclones in each pair merge, is found to be almost similar, although they might have a difference as they occur in different cyclone basins in opposite hemispheres. However, from our spatiotemporal analysis in Figs. 3–6, we can infer a few notable pieces of information:

(i) As k^{out} is high only over the cyclones, it indicates that the high incoming links in the region between two cyclones also come out from the cyclones, indicating a high vorticity interaction between both cyclones.
(ii) k^{out} values are approximately ten times larger than k^{in} in the interaction of binary cyclones. This higher magnitude of k^{out} in comparison with k^{in} indicates that stronger interactions within the networks emanate from a fewer nodes concentrated at the center of the cyclones and much less interaction with nodes farther than a certain distance from the center. However, the region of interaction in between the two cyclones has vortical connections primarily with nodes within the cyclones and is dominated by the cyclone having higher k^{out}.
(iii) A sharp decline of k^{out} outside a certain radius of the cyclones is indicative of grouping tendencies of the cyclone nodes[60] within the network.

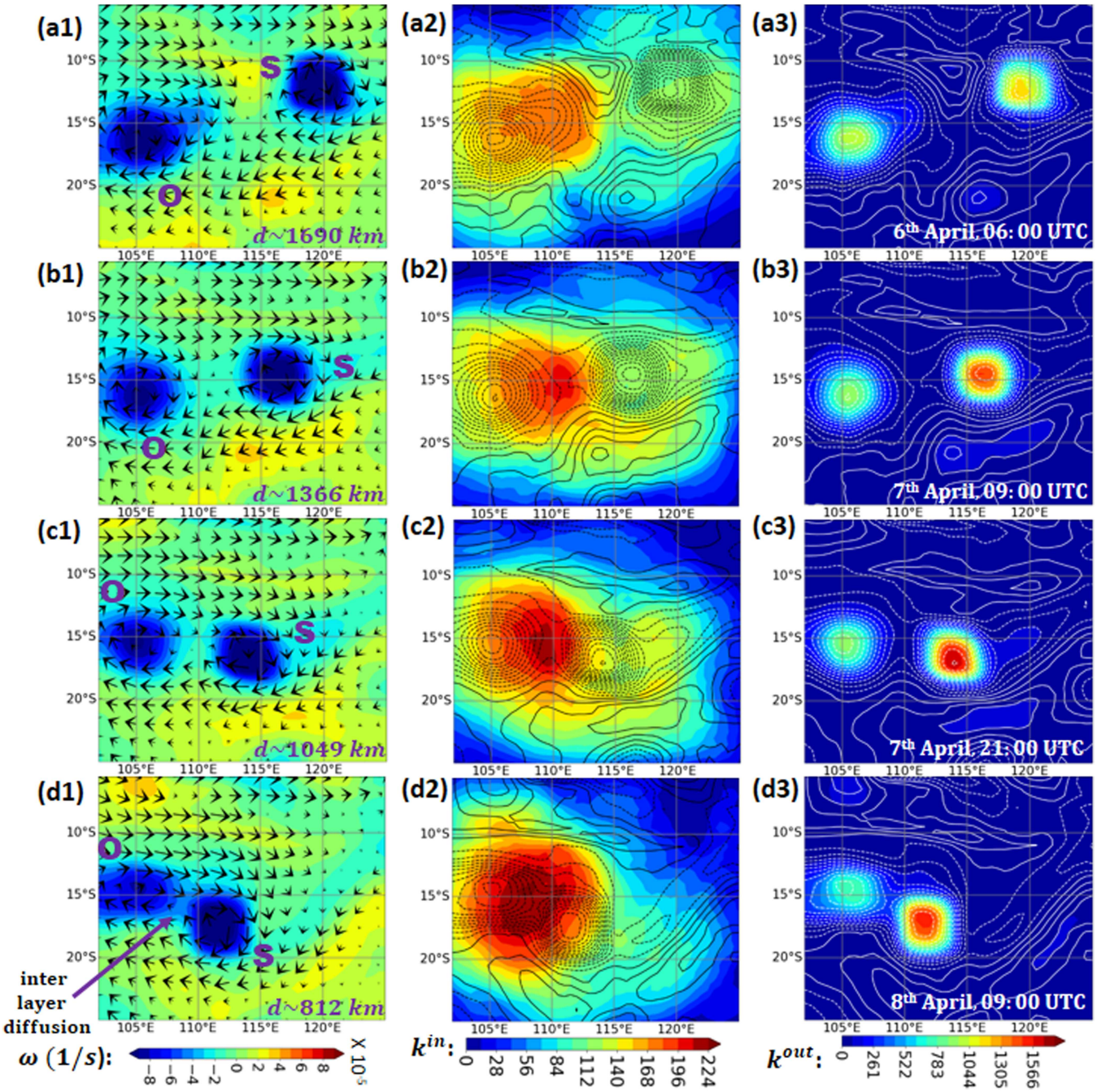

FIG. 5. The distributions of ω (a1)–(d1), k^{in} (a2)–(d2), and k^{out} (a3)–(d3) are presented during the interaction of Seroja (*S*) and Odette (*O*) at a geopotential height of 850 hPa. The time steps shown here are (a1)–(a3) 6 April 2021, 06:00 UTC; (b1)–(b3) 7 April 2021, 09:00 UTC; (c1)–(c3) 7 April 2021, 21:00 UTC; and (d1)–(d3) 8 April 2021, 09:00 UTC. The velocity vector of the wind is shown in (a1)–(d1). The vorticity contours of (a1)–(d1) are shown in the distributions of k^{in} and k^{out} for better understanding the changes of the interaction between two cyclones. Note that the negative ω is represented by the dotted line, while the portrayal of the vorticity contour by the solid line indicates the positive ω. k^{in} increases as the cyclones come closer by rotating around each other, while k^{out} of the network can explain the loss or gain of the vorticity from each cyclone during the period.

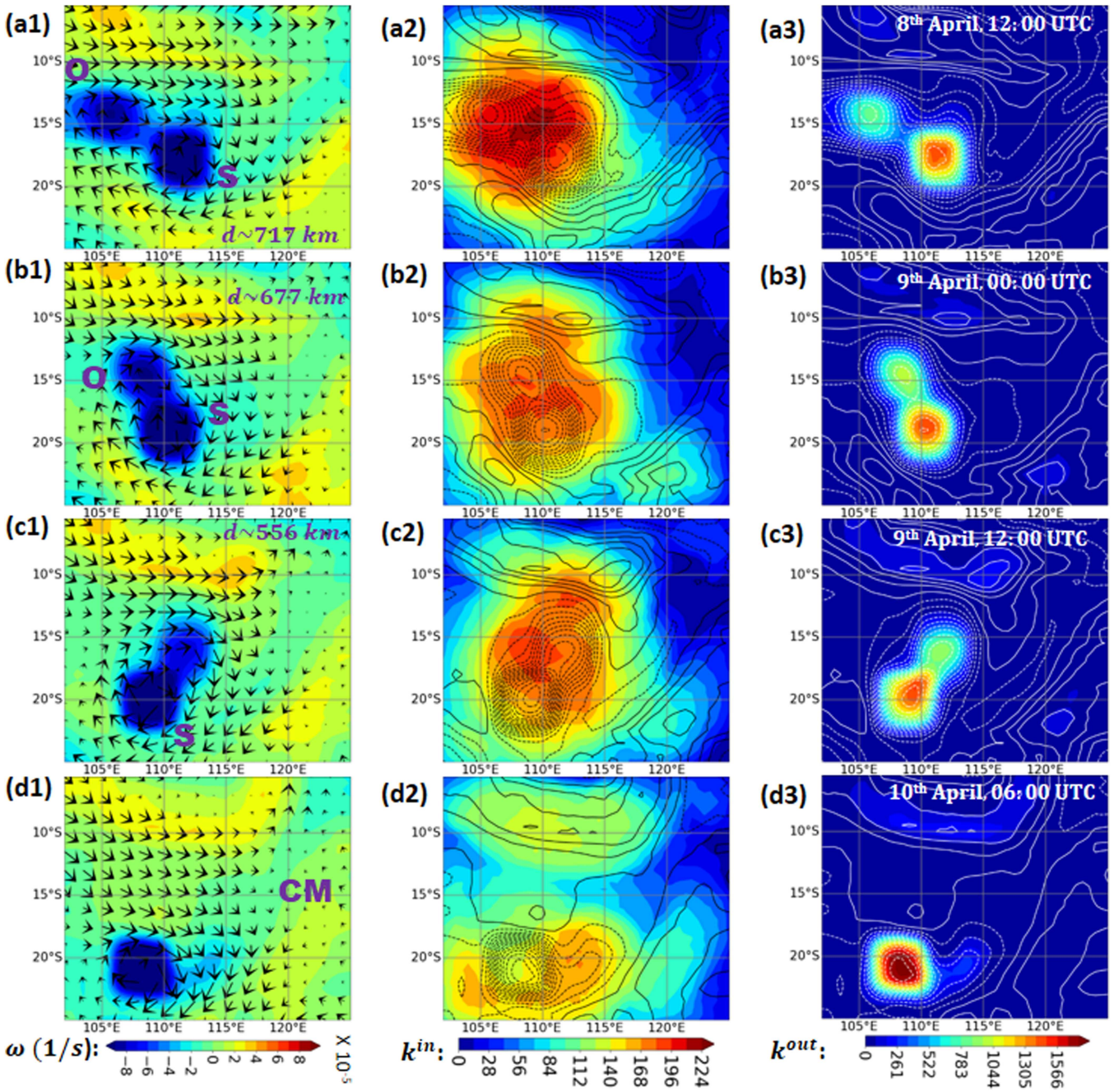

FIG. 6. The distributions of ω (a1)–(d1), k^{in} (a2)–(d2), and k^{out} (a3)–(d3) are presented during the interaction of Seroja (*S*) and Odette (*O*) prior to the CM at a geopotential height of 850 hPa. The time steps shown here are (a1)–(a3) 8 April 2021, 12:00 UTC; (b1)–(b3) 9 April 2021, 00:00 UTC; (c1)–(c3) 9 April 2021, 12:00 UTC; and (d1)–(d3) 10 April 2021, 06:00 UTC. The velocity vector of the wind is shown in (a1)–(d1). In this period, we can see a contraction of the area covered by the higher k^{in} as the interaction has a tendency to form a merged cyclone. During the CM event (d1), we can observe a higher k^{out} at the center of a merged cyclone (d3). The vorticity contours of (a1)–(d1) are shown in the distributions of k^{in} and k^{out}.

(iv) While k^{out} helps cyclones to be easily identifiable in the network topology, beyond a certain separation distance, k^{in} can be a quantitative measure of binary interaction between the two cyclones.

In Sec. III B, we test the performance of induced velocity-based network indicators in quantifying the dynamical transitions during a binary cyclone interaction leading to a CM.

B. Identification of interaction stages leading to cyclone merger

To classify the merging process into different stages, we further quantify the transitions found in the spatial distributions of the network measures by computing the mean of the 95th percentile of k^{in} ($\langle k^{in}_{95\text{th}} \rangle$), i.e., the mean of the highest 5% k^{in} in the network. To be more specific, the changes of higher k^{in} seen in the nodes located at the region between the two cyclones or inside of the weaker one [as seen in Figs. 3–6(a2)–6(d2)] enable us to characterize the transitions during the binary cyclone interaction in terms of $\langle k^{in}_{95\text{th}} \rangle$. We use the variation of $\langle k^{in}_{95\text{th}} \rangle$ during the interaction period of the two binary cyclone systems [Figs. 7(a) and 8(a1)–8(a2)]. First, we consider the variation of $\langle k^{in}_{95\text{th}} \rangle$ for the interaction between cyclones, Noru and Kulap, to distinguish the stages, leading to a cyclone merger event in Sec. III B 1. Thereafter, based on this understanding, we try to categorize the interaction between Seroja and Odette in Sec. III B 2.

1. Stages in the Noru–Kulap interaction

During the interaction between Noru and Kulap, we find stage I (23 July 2017, 03:00 UTC to 23 July 2017, 21:00 UTC) when $\langle k^{in}_{95\text{th}} \rangle$ reduces corresponding to the reduction of d between two cyclones from 1540 to 1248 km [Fig. 7(a)]. At the beginning of this stage, the peak vorticity, which is lower in the weaker cyclone (Kulap), is spread out over a larger area in comparison with Noru. As a result, during this time, we observe the highest values of k^{in} over Kulap. Furthermore, as the cyclones approach each other in this stage, the relative strength of Kulap with respect to the strength of Noru reduces. Correspondingly, the total number of connections in the network over Kulap decreases, leading to a reduction in its k^{in}. Consequently, the maximum k^{in} of the vorticity network reduces, for which we find a reduction in $\langle k^{in}_{95\text{th}} \rangle$. During this interaction period, the mutual interaction between the two cyclones is not significant due to the large d.

However, we find a rapid increase in $\langle k^{in}_{95\text{th}} \rangle$ when $d \sim 1100$ km [Fig. 7(a)]. This increment in $\langle k^{in}_{95\text{th}} \rangle$ is continuously observed until $d \sim 812$ km. We regard this interaction period (23 July 2017, 21:00 UTC to 25 July 2017, 00:00 UTC) as stage II. In this stage, we find that a high vorticity region emerges between the Noru and Kulap as a consequence of the inter-layer vorticity transport, as discussed in Sec. III A 1. In the corresponding networks, this region in between the two cyclones houses the maximum k^{in}. The vortical interactions between the two cyclones increase, leading to an increment of $\langle k^{in}_{95\text{th}} \rangle$ of the network. Furthermore, we can identify a clear distinction between stages I and II from the behavior of $\langle k^{in}_{95\text{th}} \rangle$. However, the rate of reduction of d remains the same across the two stages, and therefore, a distinction between the two stages cannot be made based on d only.

Next, after reaching its maximum value, we observe a sharp fall in $\langle k^{in}_{95\text{th}} \rangle$ from 25 July 2017, 00:00 UTC to 25 July 2017, 21:00 UTC corresponding to a relatively slower variation of d from 812

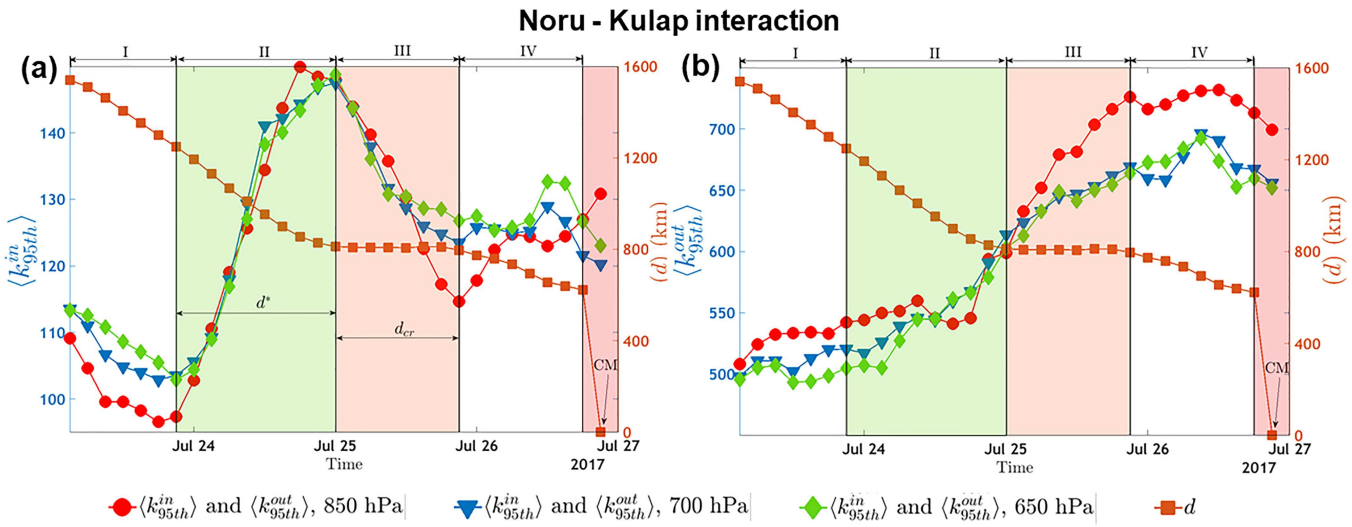

FIG. 7. (a) The variation in $\langle k^{in}_{95\text{th}} \rangle$ (mean of the 95th percentile of k^{in} in the vorticity network) for the Noru–Kulap interaction is shown. Based on the variation in $\langle k^{in}_{95\text{th}} \rangle$, we can classify this binary cyclone interaction into four stages: I, II, III, and IV, respectively. During the interaction in stages II and III, increment and reduction of $\langle k^{in}_{95\text{th}} \rangle$ indicate strengthening and weakening of the interaction between two cyclones, respectively. (b) The variation in $\langle k^{out}_{95\text{th}} \rangle$ (mean of the 95th percentile of k^{out} in the vorticity network) for the Noru–Kulap interaction is also presented here in four stages found based on the variation of $\langle k^{in}_{95\text{th}} \rangle$. The change in $\langle k^{out}_{95\text{th}} \rangle$ at each time stamp helps to quantify the variation in the strength of the dominating cyclone.

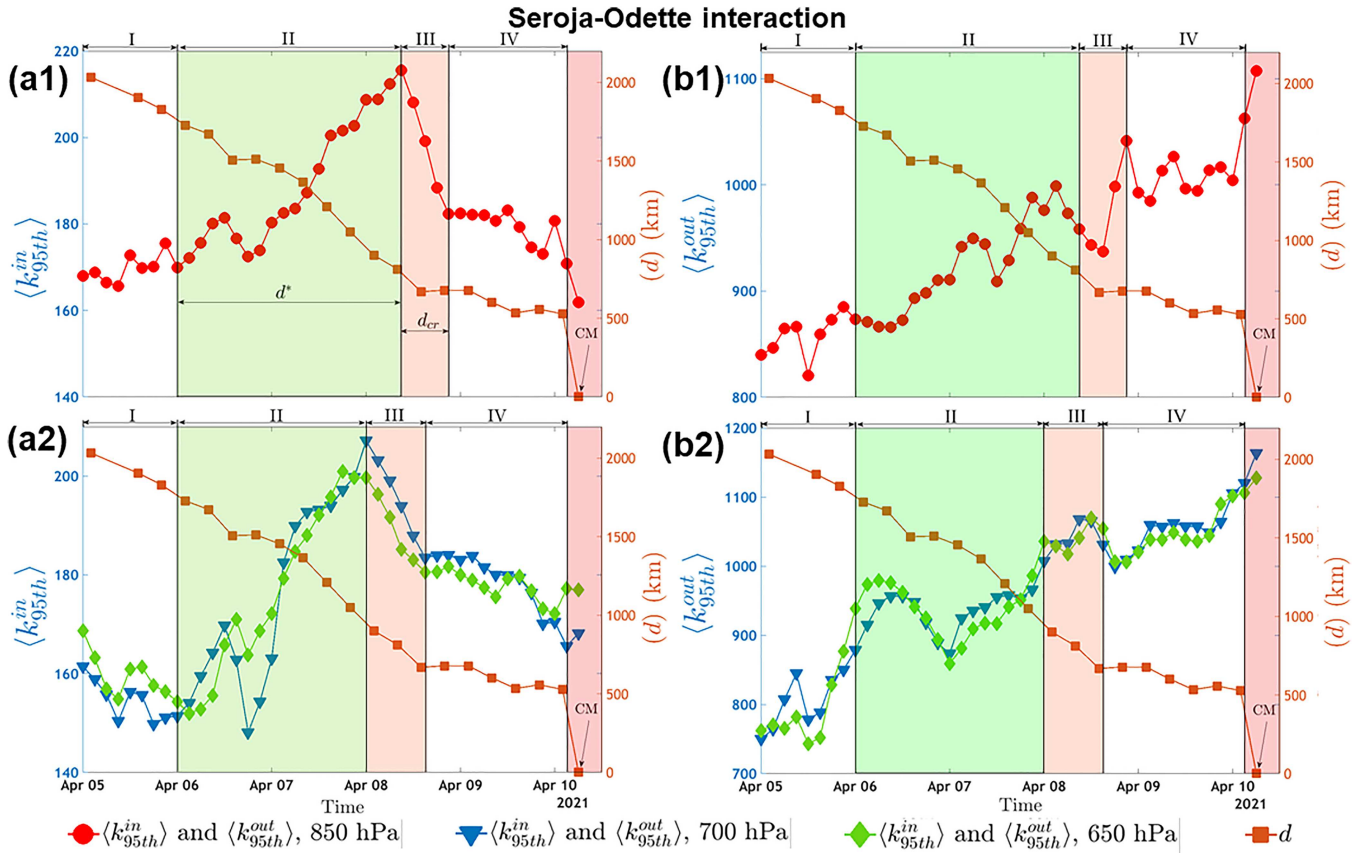

FIG. 8. (a1) The variation in $\langle k^{in}_{95th} \rangle$ (mean of 95th percentile of k^{in} in the vorticity network) for Seroja–Odette interaction is presented here at 850 hPa. (b1) The variation in $\langle k^{out}_{95th} \rangle$ for this interaction at 850 hPa is shown. (a2) and (b2) The variations of $\langle k^{in}_{95th} \rangle$ and $\langle k^{out}_{95th} \rangle$ for the same binary interaction at higher geopotential levels of 700 and 650 hPa are shown, respectively. Based on the variation of $\langle k^{in}_{95th} \rangle$, we designate four stages—I, II, III, and IV for this binary interaction.

to 797 km [Fig. 7(a)]. We refer to this period of interaction as stage III. At this stage, cyclones come in closer proximity and form a connected region of high vorticity, as shown before (Sec. III A 1). Over time, vorticity gets concentrated toward the stronger cyclone, reducing the region over which the high vorticity is distributed. Correspondingly, $\langle k^{in}_{95th} \rangle$ of the vorticity network reduces during this period.

After stage III, prior to the complete merger of Kulap into Noru, we find a relatively slower variation of $\langle k^{in}_{95th} \rangle$ (25 July 2017, 21:00 UTC to 26 July 2017, 18:00 UTC) [Fig. 7(a)]. We call this stage as stage IV. At this stage, we can see a gradual disappearance of the weaker cyclone (Kulap) [see Figs. 4(b1)–4(d1)]. Note that the mutual interaction no longer exists as Kulap gradually dies out. At this point, $\langle k^{in}_{95th} \rangle$ is determined only by the vorticity distribution in Noru and, hence, remains constant.

Hence, in total, we find four distinct stages of the Noru–Kulap interaction before the CM event. In this context, a previous study[94] discussed spontaneous formation of the coupling between two vortices of the opposite sign. However, this study primarily focused on the elementary processes of vortex pairing. Since then, a number of numerical studies[33,95] have focused on the vortex pairing and merging based on their separation distance. Recently, Cerretelli and Williamson[16] and Josserand and Rossi[33] showed different diffusion–convection stages for vortex merging based on the separation distance through experiments and numerical simulations, respectively. They found three phases before merged diffusion (or complete merging), which are first diffusion (where separation slowly reduces), convection (separation reduces rapidly), and second diffusion. However, in the present study, the stages of interaction between the two cyclones are not as distinctly demarcated by d relative to the network-based measure [Fig. 7(a)].

Furthermore, the increasing trend of $\langle k^{in}_{95th} \rangle$ in stage II [where $d = d^*$ in Fig. 7(a)] of the binary interaction denotes that $\langle k^{in}_{95th} \rangle$ is a promising tool to provide an idea of the particular separation distance beyond which the Fujiwhara interaction comes into play and give an early indication of a CM event. Furthermore, we may select a critical range of separation distance (d_{cr}) when $\langle k^{in}_{95th} \rangle$ starts to reduce (seen at stage III). After a sharp fall of $\langle k^{in}_{95th} \rangle$ in stage III, constant behavior before the merging increases the significance of d_{cr}. However, to be on the safe side, we may follow

the trend of $\langle k^{in}_{95th}\rangle$ in stage II to issue the awareness of the cyclone merging. Previously, a large number of studies[7,36] defined a threshold distance to decide whether two cyclones start to interact or not, and a separation distance within 1050–2250 km was found as the critical value for interactions of cyclones. However, estimating the separation distance to get an early indication the cyclone merger based on vorticity network-based measures proposed in the present study has a strong potential for a substantially improved forecast accuracy.

In Fig. 7(b), we compute the mean of the 95th percentile of k^{out} ($\langle k^{out}_{95th}\rangle$) for Noru–Kulap interaction to understand the changes in the influence of the dominating cyclone (Noru) at the different interaction stages. The stages obtained based on $\langle k^{in}_{95th}\rangle$ are kept the same for the analysis of $\langle k^{out}_{95th}\rangle$. During stage I, we find that the relative vorticity over Noru slowly increases at 850 hPa. Therefore, the number of vortical interactions from Noru gradually increases, leading to the increment in $\langle k^{out}_{95th}\rangle$ at 850 hPa. However, we find a small drop in the vorticity of Noru at higher geopotential levels. As a consequence of this, for a few time steps at those geopotential levels, we find a slower variation in $\langle k^{out}_{95th}\rangle$ of the vorticity network. At stage II, we find a significant increment of $\langle k^{out}_{95th}\rangle$ after its gradual increment when $d \sim 855$ km [Fig. 7(b)]. During the inter-vorticity diffusion between Noru and Kulap at this stage, the vorticity in Noru increases. As a consequence, the vortical interaction from Noru increases, leading to the increment of $\langle k^{out}_{95th}\rangle$ of the network.

At stage III [Fig. 7(b)], after the establishment of inter-layer diffusion between two cyclones, we observe a rapid increment of the relative vorticity of Noru with respect to Kulap due to the higher vorticity absorption rate of Noru (discussed in Sec. III A 1). Correspondingly, $\langle k^{out}_{95th}\rangle$ of the vorticity network rises rapidly. In stage IV [Fig. 7(b)], we find that the relative vorticity of Kulap is extremely low compared to Noru. Therefore, a further vorticity transport from Kulap to Noru does not alter the relative vorticity of Noru during this stage. As a result, the vortical connections in Noru remain almost the same throughout this stage. Consequently, we find that $\langle k^{out}_{95th}\rangle$ saturates.

In short, in stage I during Noru–Kulap interaction, we find that the variation of $\langle k^{in}_{95th}\rangle$ appears opposite to that of $\langle k^{out}_{95th}\rangle$. Note that these two network measures are observed to be higher in two different cyclones at the beginning of the interaction period. Besides, we uncover that both $\langle k^{in}_{95th}\rangle$ and $\langle k^{out}_{95th}\rangle$ increase in stage II. Therefore, a positive correlation between these two network measures can be an indication of rising interaction between two nearby cyclones. Finally, we find a saturation in both $\langle k^{in}_{95th}\rangle$ and $\langle k^{out}_{95th}\rangle$ before a complete merging event, which implies the termination of mutual interaction.

2. Stages in Seroja–Odette interaction

In Sec. III B 1, we observe the interaction stages for Noru–Kulap, which is a straightforward example of binary cyclone interaction leading to a merger. However, the classification of the stages during an interaction is not an easy task as the wind shear between the vorticity layers and wind speed at higher geopotential levels provide an additional complexity in the analysis. Therefore, to comprehend the complexity of the interaction behavior in a three-dimensional column of the atmosphere, we further investigate the stages for another binary cyclone interaction between Seroja and Odette at different geopotential heights in the present section.

At the beginning of the interaction between Seroja and Odette, we find that during stage I [5 April 2021, 00:00 UTC to 6 April 2021 00:00 UTC in Figs. 8(a1)–8(a2)], d reduces from 2034 to 1750 km due to the movement of Seroja toward Odette. Similar to the Noru–Kulap interaction, we do not identify significant mutual interaction between the two cyclones during this period as the inter-layer vorticity diffusion is not initiated for such high d. In this stage, we uncover the vorticity in the weaker cyclone (Odette) spread out over a larger area than in the stronger cyclone (Seroja). Therefore, in the beginning, as Seroja approaches Odette, we find a region of high k^{in} in and around Odette. However, we notice that the variation of $\langle k^{in}_{95th}\rangle$ is not similar to that seen for the Noru–Kulap interaction [Figs. 8(a1)–8(a2)] at this stage. During this period, Odette shows small fluctuations in vortical strength. As a consequence, the total number of connections inside Odette fluctuates, leading to the oscillations of $\langle k^{in}_{95th}\rangle$ of the network. The fluctuations in $\langle k^{in}_{95th}\rangle$ at 650 and 700 hPa are higher than those seen at 850 hPa since the area over which the vorticity of Odette is distributed significantly varies at those geopotential levels. Notably, $\langle k^{in}_{95th}\rangle$ captures this difference in the behavior between two binary cyclone interactions.

We detect an increment in $\langle k^{in}_{95th}\rangle$ when inter-layer diffusion between two cyclones starts to form stage II [Figs. 8(a1)–8(a2)], although a drop is observed before 7 April 2021, 00:00 UTC at 650, 700, and 850 hPa. However, similar to the Noru–Kulap interaction, we find an overall increasing trend of $\langle k^{in}_{95th}\rangle$ during this stage. In this stage, vorticity is transported over a large area between the two cyclones as a consequence of the formation of inter-layer vorticity diffusion, as discussed in Sec. III A 2. Therefore, the connections representing the vortical interactions are established in large numbers in this area. Consequently, $\langle k^{in}_{95th}\rangle$ increases until $d \sim 812$ km at 850 hPa and $d \sim 950$ km at 650 and 700 hPa. Note that complete formation of an inter-layer diffusion is noticed for earlier time stamps at higher geopotential levels compared to 850 hPa.

Furthermore, similar to Noru–Kulap interaction, during stage III, we find that $\langle k^{in}_{95th}\rangle$ reduces [Figs. 8(a1)–8(a2)] when the area between two cyclones over which the vorticity was spread out in stage II starts to shrink. Finally, we uncover a slower variation in $\langle k^{in}_{95th}\rangle$ as the weaker cyclone Odette starts to merge into the relatively stronger cyclone Seroja in stage IV. Hence, similar to Noru–Kulap interaction, we identify four stages during Seroja–Odette interaction.

In Figs. 8(b1)–8(b2), we estimate $\langle k^{out}_{95th}\rangle$ for Seroja–Odette interaction to characterize the influence of stronger cyclone, Seroja in stages I, II, III, and IV. We find that the vortical interaction from Seroja increases gradually toward the end of stage I as it becomes more compact and symmetric. Consequently, we notice an increment of $\langle k^{out}_{95th}\rangle$ in the network after 5 April 2021, 15:00 UTC at this stage. In stage II, we see an increasing trend of $\langle k^{out}_{95th}\rangle$ since vorticity in Seroja increases because of the gradual formation of inter-layer vorticity diffusion. However, after a complete establishment of inter-layer vorticity diffusion, we find a slight reduction in the vorticity of Seroja corresponding to an increase of vorticity inside Odette, as seen in Figs. 5(d1) and 6(a1). Consequently, we detect a small drop in $\langle k^{out}_{95th}\rangle$ on 8th April 2021, 9:00 UTC at 850 hPa

TABLE I. Details of interaction for the two binary cyclone systems, Noru–Kulap and Seroja–Odette, are summarized in this table.

Binary cyclone interaction	Factors	Stage I	Stage II	Stage III	Stage IV
Noru–Kulap	d (km)	∼1540–1248	∼1248–812	∼812–797	∼797–622
	Interaction between cyclones ($\langle k^{in}_{95th} \rangle$)	Decreases	Significantly increases	Reduces	Nearly constant
	Impact of dominating cyclone ($\langle k^{out}_{95th} \rangle$)	Slowly increases	Increases	Significantly increases	Saturates prior to CM
	Dominating cyclone	Noru	Noru	Noru	Noru
	d (km)	∼2034–1750	∼1750–812 (850 hPa) and ∼1750–950 (650 hPa & 700 hPa)	∼812–678 (850 hPa) and ∼950–670 (650 hPa & 700 hPa)	∼678–527 (850 hPa) and ∼670–527 (650 hPa & 700 hPa)
Seroja–Odette	interaction between cyclones ($\langle k^{in}_{95th} \rangle$)	nearly constant seen at 850 hPa; however exhibits successive reduction and increment at 650 and 700 hPa	Significantly increases	Significantly decreases	Nearly constant
	Impact of dominating cyclone ($\langle k^{out}_{95th} \rangle$)	Increases later in the stage	Increases	Increases after a drop during inter-layer diffusion	Again increases until CM
	Dominating cyclone	Seroja	Seroja	Seroja	Seroja

[Fig. 8(b1)], which is not observed in the case of Noru–Kulap interaction.

In stage III [Figs. 8(b1)–8(b2)], we observe a significant increase in the vorticity of Seroja due to the absorbtion of vorticity from Odette. Thus, the total vortical interactions within and from Seroja increase significantly during this stage. Consequently, $\langle k^{out}_{95th} \rangle$ of the network becomes high. However, in stage IV, in contrast to the slow alteration in the vorticity of Noru, we see a gradual increment in the vorticity of Seroja as the cyclone Odette begins to merge into it. Therefore, over this time, the total vortical interactions of Seroja gradually grow, leading to the increment of $\langle k^{out}_{95th} \rangle$ of the vorticity network [Figs. 8(b1)–8(b2)]. During the CM event, a significantly high $\langle k^{out}_{95th} \rangle$ is related to the strength of the merged cyclone, making it the dominant structure influencing the network. Overall, although we observe almost similar transitions of two binary cyclone systems from the spatiotemporal vorticity distributions (Sec. III A), we find a significant difference in the behavior of interaction during the stages based on the estimation of the network-based measures.

To summarize, the early increment in stage II (Figs. 7 and 8) makes both $\langle k^{in}_{95th} \rangle$ and $\langle k^{out}_{95th} \rangle$ promising candidates for providing vorticity interaction-based early warning signals of the CM in binary cyclone systems. On the other hand, quantification of $\langle k^{out}_{95th} \rangle$ seems to be helpful for understanding the dynamic changes of the dominating cyclone in a better way. In Table I, we have tabulated the trends at the various stages during the binary interaction of both Noru–Kulap and Seroja–Odette systems.

Thus, adopting an unweighted directed network on the relative vorticity data provides a clear perception of the transitions in the binary cyclone merging process and helps forecast the merging event.

IV. CONCLUSIONS

In this study, we explore the underlying dynamics during the interaction and complete merging of binary cyclone systems. We adopt an innovative network approach based on the pairwise induced velocity interactions among the flow elements using the Biot-Savart law to comprehend the changes in the connectivity structure during the interaction between two cyclones at their proximity. Following this framework, we perform a degree analysis of the constructed time-evolving directed induced velocity networks. The area covered by the high *in-degree* nodes in the vorticity network is observed to increase (decrease) before (after) the establishment of inter-layer diffusion between two cyclones. On the other hand, the regions with high *out-degree* of the cyclones signify that the zone of interaction between the cyclones is mainly influenced by the dominating cyclone of the binary cyclone system. Thus, using the spatial distributions of *in-degree*, we quantify the extent of binary interaction between the cyclones, while the distributions of *out-degree* help to identify the dominant cyclone during each time step of the interaction until CM.

Furthermore, a rapid fall in *out-degree*, observed after a certain distance from the periphery of each cyclone, indicates the occurrence of strong interaction within the cyclone, and thus, the distribution of *out-degree* can clearly identify the cyclone. The changes in the *out-degree* provide an insight into the vorticity interaction that is dominated by the cyclonic regions. It is noteworthy from the present study that we can classify the transitions of the binary cyclone interaction into four stages before CM occurs based on the quantification of mean of the 95th percentile of *in-degree* in the vorticity network. Besides, an early growing trend of mean of the 95th percentile of *in-degree* and mean of the 95th percentile of *out-degree* in stage-II

helps to forewarn an imminent merger event. Furthermore, these network-based measures can be used to recognize the dissimilarities in the interaction stages between different binary cyclone systems.

Thus, the complex network representation of the spatiotemporal relative vorticity field enables us to directly study the interaction structure of the vorticity field, making it a suitable approach to gain incisive insights into the interaction process of binary cyclones. Even though the Biot-Savart law is applicable strictly for velocity fields that are divergence-free, we use it to primarily estimate the strength of connection between two points in the flow field. Our results demonstrate that the measures from such a network can be effective to track various stages prior to cyclone merger. The proposed method could be further applied to study different types of cyclone interactions, such as partial merger, partial straining out, and elastic interaction in different cyclone basins. The study of the differences in the interaction structure between co-rotating and counter-rotating (such as cross-equatorial twin cyclones) cyclone pairs could also be outlined as a possible scope for future work. Furthermore, this complex network approach, in combination with the physics-inspired machine learning algorithms, can also be used to obtain a deeper understanding of the sudden track changes of cyclones caused due to the interaction of the cyclone with large-scale low-level cyclonic vortices, such as the monsoon gyre.[96] Such a detailed characterization of the connectivity structure of the different types of binary cyclones interactions is an essential step toward improving cyclone track forecasts.

ACKNOWLEDGMENTS

R.I.S. acknowledges the funding provided by the Office of Naval Research Global (Grant No. N62909-22-1-2011, contract monitor: Dr. Derrick Marcus Tepaske). S.D. would also like to acknowledge the Post Doctoral Researcher fellowship under the same grant supported by the Office of Naval Research Global at the Indian Institute of Technology Madras. S.G. and J.K. are supported by the Climate Advanced Forecasting of sub-seasonal Extremes (CAFE) project, which has received funding from the European Union's Horizon 2020 research and innovation program under the Marie Skłodowska Curie Grant Agreement No. 813844. N.M. acknowledges the BMBF grant ClimXtreme (No. 01LP1902J) "Spatial synchronization patterns of heavy precipitation events." We thank Mrs. Shruti Tandon and Dr. Gaurav Chopra for their valuable suggestions and comments for this work.

AUTHOR DECLARATIONS

Conflict of Interest

The authors have no conflicts to disclose.

Author Contributions

Somnath De: Conceptualization (equal); Data curation (equal); Formal analysis (lead); Investigation (equal); Methodology (equal); Project administration (equal); Resources (equal); Software (equal); Writing – original draft (equal); Writing – review & editing (equal). **Shraddha Gupta:** Conceptualization (equal); Formal analysis (supporting); Investigation (equal); Methodology (equal); Resources (equal); Writing – original draft (equal); Writing – review & editing (equal). **Vishnu R. Unni:** Conceptualization (equal); Formal analysis (supporting); Investigation (equal); Methodology (equal); Writing – review & editing (equal). **Rewanth Ravindran:** Data curation (equal); Methodology (equal); Software (equal). **Praveen Kasthuri:** Conceptualization (equal); Formal analysis (supporting); Investigation (equal); Methodology (equal); Resources (equal); Writing – review & editing (equal). **Norbert Marwan:** Conceptualization (equal); Methodology (equal); Resources (equal); Supervision (equal); Writing – review & editing (equal). **Jürgen Kurths:** Conceptualization (equal); Methodology (equal); Resources (equal); Supervision (equal); Writing – review & editing (equal). **R. I. Sujith:** Conceptualization (equal); Formal analysis (supporting); Funding acquisition (lead); Investigation (equal); Methodology (equal); Project administration (equal); Resources (equal); Supervision (equal); Writing – review & editing (equal).

DATA AVAILABILITY

The data/reanalysis that support the findings of this study are openly available in Copernicus at https://cds.climate.copernicus.eu/ (ERA5 reanalysis data; last accessed 16 December 2021), Ref. 63. For tracking the coordinates of the cyclone, we use Weather Underground's online database (https://www.wunderground.com/hurricane; last accessed on 20 December 2021), Ref. 88.

APPENDIX: CALCULATION STEPS FOR ESTIMATING THE SEPARATION DISTANCE

The following equations (A1)–(A3) are used to calculate the separation distance between two nearby cyclones in the present work:

$$B_1 = \sin^2\frac{\delta\phi}{2} + \cos\phi_1 * \cos\phi_2 * \sin^2\frac{\delta\theta}{2}. \tag{A1}$$

Here, ϕ_1 and ϕ_2 are the latitudes of two cyclones at a particular time instance. We calculate the difference in the latitude, $\delta\phi = \phi_1 - \phi_2$. Similarly, $\delta\theta$ is the difference in the longitude of two corresponding cyclones,

$$B_2 = 2\tan^{-1}\left(\sqrt{B1}, \sqrt{1-B1}\right). \tag{A2}$$

The separation distance between two cyclones can be calculated as

$$d = R * B_2. \tag{A3}$$

REFERENCES

[1] A. H. Fink and P. Speth, "Tropical cyclones," Naturwissenschaften **85**, 482–493 (1998).
[2] T. Knutson, S. J. Camargo, J. C. Chan, K. Emanuel, C.-H. Ho, J. Kossin, M. Mohapatra, M. Satoh, M. Sugi, K. Walsh, and L. Wu, "Tropical cyclones and climate change assessment: Part I: Detection and attribution," Bull. Am. Meteorol. Soc. **100**, 1987–2007 (2019).
[3] T. Okada, "Kisyogaku kowa," in Manual of Meteorology Lecture on Meteorology, 1907.
[4] S. Fujiwhara, "On the growth and decay of vortical systems," Q. J. R. Meteorol. Soc. **49**, 75–104 (1923).
[5] S. Fujiwhara, "Short note on the behavior of two vortices," Proc. Phys. Math. Soc. Jpn. 3rd Ser. **13**, 106–110 (1931).

[6]S. Fujiwhara, "The natural tendency towards symmetry of motion and its application as a principle in meteorology," Q. J. R. Meteorol. Soc. **47**, 287–292 (1921).
[7]Y.-A. Liou, J.-C. Liu, M.-X. Wu, Y.-J. Lee, C.-H. Cheng, C.-P. Kuei, and R.-M. Hong, "Generalized empirical formulas of threshold distance to characterize cyclone–cyclone interactions," IEEE Trans. Geosci. Remote Sens. **54**, 3502–3512 (2016).
[8]J.-C. Liu, Y.-A. Liou, M.-X. Wu, Y.-J. Lee, C.-H. Cheng, C.-P. Kuei, and R.-M. Hong, "Analysis of interactions among two tropical depressions and typhoons Tembin and Bolaven (2012) in Pacific Ocean by using satellite cloud images," IEEE Trans. Geosci. Remote Sens. **53**, 1394–1402 (2014).
[9]E. W. Hoover, "Relative motion of hurricane pairs," Mon. Weather Rev. **89**, 251–255 (1961).
[10]Y.-A. Liou and R. S. Pandey, "Interactions between typhoons Parma and Melor (2009) in North West Pacific Ocean," Weather Clim. Extremes **29**, 100272 (2020).
[11]See https://earthobservatory.nasa.gov/images/148180/seroja-slams-australia?src=eoa-iotd for "Seroja Slams Australia" (2021) (last accessed June 4, 2022).
[12]Y.-A. Liou, J.-C. Liu, C.-C. Liu, C.-H. Chen, K.-A. Nguyen, and J. P. Terry, "Consecutive dual-vortex interactions between quadruple typhoons Noru, Kulap, Nesat and Haitang during the 2017 North Pacific typhoon season," Remote Sens. **11**, 1843 (2019).
[13]R. Prieto, B. D. McNoldy, S. R. Fulton, and W. H. Schubert, "A classification of binary tropical cyclone-like vortex interactions," Mon. Weather Rev. **131**, 2656–2666 (2003).
[14]T. Leweke, S. Le Dizes, and C. H. Williamson, "Dynamics and instabilities of vortex pairs," Annu. Rev. Fluid Mech. **48**, 507–541 (2016).
[15]P. Meunier, S. Le Dizes, and T. Leweke, "Physics of vortex merging," C.R. Phys. **6**, 431–450 (2005).
[16]C. Cerretelli and C. Williamson, "The physical mechanism for vortex merging," J. Fluid Mech. **475**, 41–77 (2003).
[17]S. Brand, "Interaction of binary tropical cyclones of the western North Pacific Ocean," J. Appl. Meteorol. Climatol. **9**, 433–441 (1970).
[18]L. E. Carr and R. L. Elsberry, "Dynamical tropical cyclone track forecast errors. Part I: Tropical region error sources," Weather Forecast. **15**, 641–661 (2000).
[19]E.-J. Cha, S. gyeong Yun, I.-J. Moon, and D.-H. Kim, "Binary interaction of typhoons Soulik and Cimaron in 2018—Part I: Observational characteristics and forecast error," Trop. Cyclone Res. Rev. **10**, 32–42 (2021).
[20]See https://www.metoc.navy.mil/jtwc/products/atcr/2012atcr.pdf for "Annual Tropical Cyclone Report," Joint Typhoon Warning Center (JTWC) (2012) (last accessed Febuary 22, 2022).
[21]K. Dong and C. J. Neumann, "On the relative motion of binary tropical cyclones," Mon. Weather Rev. **111**, 945–953 (1983).
[22]M. Lander and G. J. Holland, "On the interaction of tropical-cyclone-scale vortices. I: Observations," Q. J. R. Meteorol. Soc. **119**, 1347–1361 (1993).
[23]C. K. Tang, J. C. Chan, and M. Yamaguchi, "Large tropical cyclone track forecast errors of global numerical weather prediction models in western North Pacific basin," Trop. Cyclone Res. Rev. **10**, 151–169 (2021).
[24]E. A. Ritchie and G. J. Holland, "On the interaction of tropical-cyclone-scale vortices. II: Discrete vortex patches," Q. J. R. Meteorol. Soc. **119**, 1363–1379 (1993).
[25]J. Liang and L. Wu, "Sudden track changes of tropical cyclones in monsoon gyres: Full-physics, idealized numerical experiments," J. Atmos. Sci. **72**, 1307–1322 (2015).
[26]S. Wei-Jen Chang, "A numerical study of the interactions between two tropical cyclones," Mon. Weather Rev. **111**, 1806–1817 (1983).
[27]M. DeMaria and J. C. Chan, "Comments on 'A numerical study of the interactions between two tropical cyclones,'" Mon. Weather Rev. **112**, 1643–1645 (1984).
[28]K. Roberts and J. Christiansen, "Topics in computational fluid mechanics," Comput. Phys. Commun. **3**, 14–32 (1972).
[29]P. Saffman and R. Szeto, "Equilibrium shapes of a pair of equal uniform vortices," Phys. Fluids **23**, 2339–2342 (1980).
[30]E. A. Overman and N. J. Zabusky, "Evolution and merger of isolated vortex structures," Phys. Fluids **25**, 1297–1305 (1982).
[31]D. G. Dritschel, "The nonlinear evolution of rotating configurations of uniform vorticity," J. Fluid Mech. **172**, 157–182 (1986).
[32]P. Meunier, U. Ehrenstein, T. Leweke, and M. Rossi, "A merging criterion for two-dimensional co-rotating vortices," Phys. Fluids **14**, 2757–2766 (2002).
[33]C. Josserand and M. Rossi, "The merging of two co-rotating vortices: A numerical study," Eur. J. Mech. B Fluids **26**, 779–794 (2007).
[34]G. J. Holland and G. S. Dietachmayer, "On the interaction of tropical-cyclone-scale vortices. III: Continuous barotropic vortices," Q. J. R. Meteorol. Soc. **119**, 1381–1398 (1993).
[35]C.-C. Wu, T.-S. Huang, W.-P. Huang, and K.-H. Chou, "A new look at the binary interaction: Potential vorticity diagnosis of the unusual southward movement of tropical storm Bopha (2000) and its interaction with supertyphoon Saomai (2000)," Mon. Weather Rev. **131**, 1289–1300 (2003).
[36]J. Liu, Y. Liou, M. Wu, Y. Lee, C. Cheng, C. Kuei, and R. Hong, "Interactions among two tropical depressions and typhoons Tembin and Bolaven (2012) in Pacific Ocean: Analysis of the depression-cyclone interactions with 3-D reconstruction of satellite cloud images," IEEE Trans. Geosci. Remote Sens. **53**, 1394–1402 (2015).
[37]L. Li and X. Ge, "Intensity change of Noru (2017) during binary tropical cyclones interaction," Asia-Pac. J. Atmos. Sci. **57**, 135–147 (2021).
[38]A. Benfield, See http://thoughtleadership.aon.com for "Global Catastrophe Recap August 2017" (accessed May 11, 2022).
[39]J. Nott, "A 6000 year tropical cyclone record from Western Australia," Quat. Sci. Rev. **30**, 713–722 (2011).
[40]S. H. Strogatz, "Exploring complex networks," Nature **410**, 268–276 (2001).
[41]M. E. Newman, "The structure and function of complex networks," SIAM Rev. **45**, 167–256 (2003).
[42]E. de Silva and M. P. Stumpf, "Complex networks and simple models in biology," J. R. Soc. Interface **2**, 419–430 (2005).
[43]D. Krioukov, M. Kitsak, R. S. Sinkovits, D. Rideout, D. Meyer, and M. Boguñá, "Network cosmology," Sci. Rep. **2**, 793 (2012).
[44]A.-L. Barabási, "Network science," Philos. Trans. R. Soc. A: Math. Phys. Eng. Sci. **371**, 20120375 (2013).
[45]A. Krishnan, R. Sujith, N. Marwan, and J. Kurths, "Suppression of thermoacoustic instability by targeting the hubs of the turbulent networks in a bluff body stabilized combustor," J. Fluid Mech. **916**, A20 (2021).
[46]A. A. Tsonis and P. J. Roebber, "The architecture of the climate network," Physica A **333**, 497–504 (2004).
[47]J. F. Donges, Y. Zou, N. Marwan, and J. Kurths, "Complex networks in climate dynamics," Eur. Phys. J. Spec. Top. **174**, 157–179 (2009).
[48]J. F. Donges, Y. Zou, N. Marwan, and J. Kurths, "The backbone of the climate network," Europhys. Lett. **87**, 48007 (2009).
[49]N. Marwan and J. Kurths, "Complex network based techniques to identify extreme events and (sudden) transitions in spatio-temporal systems," Chaos **25**, 097609 (2015).
[50]J. Meng, J. Fan, Y. Ashkenazy, and S. Havlin, "Percolation framework to describe El Niño conditions," Chaos **27**, 035807 (2017).
[51]N. Ekhtiari, A. Agarwal, N. Marwan, and R. V. Donner, "Disentangling the multi-scale effects of sea-surface temperatures on global precipitation: A coupled networks approach," Chaos **29**, 063116 (2019).
[52]V. Stolbova, P. Martin, B. Bookhagen, N. Marwan, and J. Kurths, "Topology and seasonal evolution of the network of extreme precipitation over the Indian subcontinent and Sri Lanka," Nonlinear Process. Geophys. **21**, 901–917 (2014).
[53]N. Malik, B. Bookhagen, N. Marwan, and J. Kurths, "Analysis of spatial and temporal extreme monsoonal rainfall over South Asia using complex networks," Clim. Dyn. **39**, 971–987 (2012).
[54]V. Stolbova, E. Surovyatkina, B. Bookhagen, and J. Kurths, "Tipping elements of the Indian monsoon: Prediction of onset and withdrawal," Geophys. Res. Lett. **43**, 3982–3990, https://doi.org/10.1002/2016GL068392 (2016).
[55]N. Boers, B. Bookhagen, N. Marwan, J. Kurths, and J. Marengo, "Complex networks identify spatial patterns of extreme rainfall events of the South American monsoon system," Geophys. Res. Lett. **40**, 4386–4392, https://doi.org/10.1002/grl.50681 (2013).
[56]N. Boers, B. Bookhagen, J. Marengo, N. Marwan, J.-S. von Storch, and J. Kurths, "Extreme rainfall of the South American monsoon system: A dataset comparison using complex networks," J. Clim. **28**, 1031–1056 (2015).

[57]N. Boers, B. Goswami, A. Rheinwalt, B. Bookhagen, B. Hoskins, and J. Kurths, "Complex networks reveal global pattern of extreme-rainfall teleconnections," Nature **566**, 373–377 (2019).
[58]J. Ludescher, M. Martin, N. Boers, A. Bunde, C. Ciemer, J. Fan, S. Havlin, M. Kretschmer, J. Kurths, J. Runge, V. Stolbova, E. Surovyatkina, and H. J. Schellnhuber, "Network-based forecasting of climate phenomena," Proc. Natl. Acad. Sci. U.S.A. **118**, e1922872118 (2021).
[59]N. Boers, J. Kurths, and N. Marwan, "Complex systems approaches for Earth system data analysis," J. Phys.: Complex. **2**, 011001 (2021).
[60]S. Gupta, N. Boers, F. Pappenberger, and J. Kurths, "Complex network approach for detecting tropical cyclones," Clim. Dyn. **57**, 3355–3364 (2021).
[61]K. Taira, A. G. Nair, and S. L. Brunton, "Network structure of two-dimensional decaying isotropic turbulence," J. Fluid Mech. **795**, R2 (2016).
[62]J. Fan, J. Meng, J. Ludescher, X. Chen, Y. Ashkenazy, J. Kurths, S. Havlin, and H. J. Schellnhuber, "Statistical physics approaches to the complex Earth system," Phys. Rep. **896**, 1–84 (2021).
[63]H. Hersbach, B. Bell, P. Berrisford, S. Hirahara, A. Horányi, J. Muñoz-Sabater, J. Nicolas, C. Peubey, R. Radu, D. Schepers, A. Simmons, C. Soci, S. Abdalla, X. Abellan, G. Balsamo, P. Bechtold, G. Biavati, J. Bidlot, M. Bonavita, G. Chiara, P. Dahlgren, D. Dee, M. Diamantakis, R. Dragani, J. Flemming, R. Forbes, M. Fuentes, A. Geer, L. Haimberger, S. Healy, R. J. Hogan, E. Hölm, M. Janisková, S. Keeley, P. Laloyaux, P. Lopez, C. Lupu, G. Radnoti, P. Rosnay, I. Rozum, F. Vamborg, S. Villaume, and J. Thépaut, "The ERA5 global reanalysis," Q. J. R. Meteorol. Soc. **146**, 1999–2049 (2020).
[64]C. Lam and S. Lai, "Use of ECMWF 850-hPa vorticity fields in the forecasting of tropical cyclones and intense lows in June-July 1994," in *Proceedings of 9th Guangdong-Hong Kong-Macau Joint Seminar on Hazardous Weather* (Hong Kong Observatory, 1994), pp. 137–156.
[65]E. Flaounas, V. Kotroni, K. Lagouvardos, and I. Flaounas, "Cyclotrack (v1.0)–tracking winter extratropical cyclones based on relative vorticity: Sensitivity to data filtering and other relevant parameters," Geosci. Model Dev. **7**, 1841–1853 (2014).
[66]S. Chen, W. Li, Y. Lu, and Z. Wen, "Variations of latent heat flux during tropical cyclones over the South China sea," Meteorol. Appl. **21**, 717–723 (2014).
[67]Y. Wu, S. Chen, W. Li, R. Fang, and H. Liu, "Relative vorticity is the major environmental factor controlling tropical cyclone intensification over the Western North Pacific," Atmos. Res. **237**, 104874 (2020).
[68]W. M. Gray, "Global view of the origin of tropical disturbances and storms," Mon. Weather Rev. **96**, 669–700 (1968).
[69]J. Kouroutzoglou, H. Flocas, I. Simmonds, K. Keay, and M. Hatzaki, "Assessing characteristics of Mediterranean explosive cyclones for different data resolution," Theor. Appl. Climatol. **105**, 263–275 (2011).
[70]S.-S. Ho and A. Talukder, "Cyclone tracking using multiple satellite data sources via spatial-temporal knowledge transfer," in *AAAI-08 Workshop, Transfer Learning for Complex Tasks* (AAAI Press, 2008).
[71]J. Molinari, D. Vollaro, and F. Robasky, "Use of ECMWF operational analyses for studies of the tropical cyclone environment," Meteorol. Atmos. Phys. **47**, 127–144 (1992).
[72]M. T. Pillay and J. M. Fitchett, "On the conditions of formation of Southern Hemisphere tropical cyclones," Weather Clim. Extremes **34**, 100376 (2021).
[73]C. Neumann, "Use of deep-layer mean geopotential height fields in statistical prediction of tropical cyclone motion," Bull. Am. Meteorol. Soc. **60**, 584 (1979).
[74]T. B. Kimberlain and M. J. Breman, "Tropical cyclone motion," in *Global Guide to Tropical Cyclone Forecasting* (World Meteorological Organization, 2017), pp. 63–155.
[75]C. S. Velden and L. M. Leslie, "The basic relationship between tropical cyclone intensity and the depth of the environmental steering layer in the Australian region," Weather Forecast. **6**, 244–253 (1991).
[76]R. Sujith and V. R. Unni, "Complex system approach to investigate and mitigate thermoacoustic instability in turbulent combustors," Phys. Fluids **32**, 061401 (2020).
[77]R. De Regt, S. Apunevych, C. Von Ferber, Y. Holovatch, and B. Novosyadlyj, "Network analysis of the COSMOS galaxy field," Mon. Not. R. Astron. Soc. **477**, 4738–4748 (2018).
[78]G. R. Ávila, A. Gapelyuk, N. Marwan, H. Stepan, J. Kurths, T. Walther, and N. Wessel, "Classifying healthy women and preeclamptic patients from cardiovascular data using recurrence and complex network methods," Auton. Neurosci. **178**, 103–110 (2013).
[79]L. Chen, N. Blumm, N. Christakis, A. Barabasi, and T. S. Deisboeck, "Cancer metastasis networks and the prediction of progression patterns," Br. J. Cancer **101**, 749–758 (2009).
[80]K. F. Davis, P. D'Odorico, F. Laio, and L. Ridolfi, "Global spatio-temporal patterns in human migration: A complex network perspective," PLoS One **8**, e53723 (2013).
[81]S. Boccaletti, V. Latora, Y. Moreno, M. Chavez, and D.-U. Hwang, "Complex networks: Structure and dynamics," Phys. Rep. **424**, 175–308 (2006).
[82]S. Abe and N. Suzuki, "Scale-free network of earthquakes," Europhys. Lett. **65**, 581 (2004).
[83]S. Scarsoglio, F. Laio, and L. Ridolfi, "Climate dynamics: A network-based approach for the analysis of global precipitation," PLoS One **8**, e71129 (2013).
[84]M. G. Meena and K. Taira, "Identifying vortical network connectors for turbulent flow modification," J. Fluid Mech. **915**, A10 (2021).
[85]J. D. Jackson, *Classical Electrodynamics*, 3rd ed. (John Wiley & Sons, 1999), 808 pp., ISBN: 0-471-30932-X.
[86]R. Shankar, *Fundamentals of Physics II* (Yale University Press, 2016).
[87]J. D. Anderson, in *Fundamentals of Aerodynamics* (McGraw, 2009).
[88]See https://www.wunderground.com/hurricane for "Hurricane and Tropical Cyclones" (last accessed December 20, 2021).
[89]N. R. Chopde and M. Nichat, "Landmark based shortest path detection by using A* and Haversine formula," Int. J. Innov. Res. Comput. Commun. Eng. **1**, 298–302 (2013).
[90]B. J. Hoskins and K. I. Hodges, "New perspectives on the Northern Hemisphere winter storm tracks," J. Atmos. Sci. **59**, 1041–1061 (2002).
[91]C. Cerretelli and C. H. Williamson, "A new family of uniform vortices related to vortex configurations before merging," J. Fluid Mech. **493**, 219–229 (2003).
[92]See "The Coriolis Effect: Earth's Rotation and Its Effect on Weather" for https://www.nationalgeographic.org/encyclopedia/coriolis-effect/4th-grade/ (last accessed April 4, 2022).
[93]F. Khadami and D. W. Purnaningtyas, "Ocean response to tropical cyclone Seroja at East Nusa Tenggara waters," IOP Conf. Ser.: Earth Environ. Sci. **925**, 012045 (2021).
[94]Y. Couder and C. Basdevant, "Experimental and numerical study of vortex couples in two-dimensional flows," J. Fluid Mech. **173**, 225–251 (1986).
[95]L. K. Brandt and K. K. Nomura, "The physics of vortex merger and the effects of ambient stable stratification," J. Fluid Mech. **592**, 413–446 (2007).
[96]K. Song, L. Tao, and J. Gao, "Rapid weakening of tropical cyclones in monsoon gyres over the Western North Pacific: A revisit," Front. Earth Sci. **9**, 507 (2021).